View metadata, citation and similar papers at core.ac.uk

brought to you by CORE

provided by NASA Technical Reports Server

NASA TECHNICAL MEMORANDUM

NASA TM X-3195

NASA TM X-3195

(NASA-TM-X-3195) PERFORMANCE OF VORTEX GENERATORS IN A MACH 2.5 LOW-BLEED FULL SCALE 45-PERCENT-INTERNAL-CONTRACTION AXISYMMETRIC INLET (NASA) 45 p HC $3.75 N75-20335

CSCL 20D H1/07 Unclas 18188

PERFORMANCE OF VORTEX GENERATORS IN A MACH 2.5 LOW-BLEED FULL-SCALE 45-PERCENT-INTERNAL-CONTRACTION AXISYMMETRIC INLET

Harvey E. Neumann, Joseph F. Wasserbauer, and Robert J. Shaw

Lewis Research Center

Cleveland, Ohio 44135

NATIONAL AERONAUTICS AND SPACE ADMINISTRATION • WASHINGTON, D. C. • APRIL 1975

1. Report No NASA TM X-3195	2. Government Accession No	3. Recipient's Catalog No
4. Title and Subtitle PERFORMANCE OF VORTEX GENERATORS IN A MACH 2.5 LOW-BLEED FULL-SCALE 45-PERCENT-INTERNAL-CONTRACTION AXISYMMETRIC INLET		5. Report Date April 1975 6. Performing Organization Code
7. Author(s) Harvey E. Neumann, Joseph F. Wasserbauer, and Robert J. Shaw		8. Performing Organization Report No E-8117 10. Work Unit No 505-04
9. Performing Organization Name and Address Lewis Research Center National Aeronautics and Space Administration Cleveland, Ohio 44135		11. Contract or Grant No 13. Type of Report and Period Covered Technical Memorandum
12. Sponsoring Agency Name and Address National Aeronautics and Space Administration Washington, D.C. 20546		14. Sponsoring Agency Code

15. Supplementary Notes

16. Abstract

Steady-state and dynamic flow characteristics associated with two sets of vortex generators having different mixing criteria were determined. The inlet performance with and without these vortex generators is presented. The vortex generators were successful in eliminating separation, increasing area-weighted total pressure recovery, and decreasing distortion. Transmission times obtained from cross-correlations of the wall static pressures and the diffuser exit total pressure showed no effect of the upstream flow characteristics on the diffuser exit pressures when generators were used. Without generators, separation occurred and the upstream pressure characteristics had immediate effects on the diffuser exit pressure characteristics.

17. Key Words (Suggested by Author(s)) Supersonic cruise inlets Inlets Propulsion systems	18. Distribution Statement Unclassified - unlimited STAR category 07 (rev.)		
19. Security Classif. (of this report) Unclassified	20. Security Classif. (of this page) Unclassified	21. No. of Pages 44	22. Price* $3.75

* For sale by the National Technical Information Service, Springfield, Virginia 22151

PERFORMANCE OF VORTEX GENERATORS IN A MACH 2.5 LOW-BLEED FULL-SCALE 45-PERCENT-INTERNAL-CONTRACTION AXISYMMETRIC INLET

by Harvey E. Neumann, Joseph F. Wasserbauer, and Robert J. Shaw

Lewis Research Center

SUMMARY

An experimental investigation was made to determine the effects of two sets of vortex generators on the total pressure recovery and distortion at the subsonic diffuser exit of an axisymmetric mixed-compression supersonic inlet. The dynamic flow characteristics associated with the vortex generators were also investigated. The two sets of vortex generators were similar in design and differed primarily in their chord and aspect ratio. This geometry difference resulted in the vortex generators having different mixing criteria. The inlet was designed for Mach 2.5 operation. The external compression was provided by a bicone centerbody having half-angles of 12.5° and 18.5°. Forty-five percent of the supersonic area contraction occurred internally.

Data were obtained at two Mach numbers: 2.5 and 2.0. The Reynolds number at both Mach numbers was 8.2 million per meter.

Steady-state total pressure surveys were made at the subsonic diffuser entrance and exit and two locations within the diffuser. Measurements were made of the fluctuating component of wall static pressure up- and downstream of the vortex generators and of the fluctuating component of total pressure at the diffuser exit. These measurements were used to investigate auto- and cross-correlations of the fluctuating pressures.

With no vortex generators the flow separated in the subsonic diffuser. The separation adversely affected the total pressure recovery and distortion at the diffuser exit. Both sets of vortex generators tested were successful in eliminating this separation. Area-weighted total pressure recovery was therefore increased and steady-state distortion was reduced. The vortex generators with the smaller chord and aspect ratio were the most efficient.

The signal transmission paths associated with the dynamics of the flow near the vortex generators and the diffuser exit were studied. Without vortex generators, the diffuser flow was separated. The correlation function coefficient indicated that the flow at the diffuser exit was then immediately influenced by the dynamics of the flow near the vortex generators. The vortex action of the generators wiped out all effect of upstream pressure on the diffuser exit pressure. The correlation function coefficient indicated no single source of influence at the diffuser exit. Thus, the fluctuating pressure signal at the diffuser exit was influenced by other signals beyond the scope of this investigation.

INTRODUCTION

It has long been recognized that flow separation and relatively large pressure distortions at the engine face are problems associated with supersonic inlets, particularly those incorporating short diffusers. Boundary layer bleed can be used to prevent flow separation and thus to reduce distortion but not without incurring drag penalties. Vortex generators are therefore commonly used as an additional boundary layer control device because they may not experience as severe a drag penalty as increased performance bleed.

The performance of vortex generators and their ability to mix the high-energy air with the low-energy boundary layer have been extensively studied in references 1 and 2. Most of the past experimental tests with vortex generators have been concerned with only the steady-state flow characteristics within the diffuser. Time-varying pressures are generally determined only at the diffuser exit (ref. 3). These fluctuating pressures are of importance inasmuch as they are superimposed upon the steady-state distortion. If the vortex action has not sufficiently dissipated at the engine face, the resultant instantaneous distortions can be expected to adversely affect the stall margin of an engine. The present study was therefore undertaken in the Lewis 10- by 10-Foot Supersonic Wind Tunnel to define the character of the pressure fluctuations associated with the vortex generators used in the design of the very-low-bleed, mixed-compression inlet of references 4 and 5. Two sets of vortex generators having different chords were selected for study. The steady-state performance of the vortex generators, in terms of energizing the boundary layer and improving the inlet pressure recovery and distortion characteristics, was also determined. The time-varying pressure characteristics were evaluated by a study of the auto- and cross-correlations of the pressure fluctuations across the vortex generators. The test was conducted at Mach numbers of 2.5 and 2.0 and a Reynolds number of 8.2 million per meter.

U.S. customary units were used in the recording and computing of experimental data. These units were converted to the International System of Units (SI) for presentation in this report.

APPARATUS AND PROCEDURE

Model

The model installed in the NASA Lewis 10- by 10-Foot Supersonic Wind Tunnel is shown in figure 1(a). The inlet used in this investigation was designed for operation at Mach 2.5. The flow capacity of the inlet was sized for operation with a TF30-P-3 turbofan engine at Mach 2.5. For this study, however, the inlet was coupled to a cold-pipe -

choked-plug assembly. Figure 1(b) shows the inlet nacelle combination mounted from the vertical strut in the wind tunnel test section.

The details of the inlet design are given in figure 2. Figure 2(a) is an isometric view of the inlet. The essential features of the inlet were a bicone centerbody of 12.5° and 18.5° half-angle cones and an initial internal cowl angle of 2° (fig. 2(b)). The details of the inlet design are given in references 4 and 5. The design philosophy for this axisymmetric, mixed-compression inlet was to utilize a bicone spike to provide the maximum external compression compatible with high total pressure recovery and low cowl drag. As a result, 45 percent of the supersonic area contraction was internal for the Mach 2.5 design condition.

In order to vary contraction ratio, the design philosophy provided for a collapsing centerbody. The second cone would be collapsed in its lowest position to blend into the first cone and the diffuser centerbody contour so as to form a single conic centerbody. For economic reasons the mechanical design of the test inlet was simplified so that the contraction ratio was varied at each test Mach number by centerbody translation rather than by collapsing. A second centerbody whose second cone angle was 14.5° was designed as the collapsed version for operation at Mach 2.0 (fig. 2(b)).

The boundary layer development in the inlet was controlled by performance bleed. Provision for cowl boundary layer bleed was made by using perforated surfaces both forward and aft of the geometric throat (figs. 2(a) and (b)). These cowl bleed perforations were sealed for the tests presented herein. The two centerbody performance bleed configurations used are shown in figures 2(c) and (d). Sharp-lip configuration D was used in all tests reported herein with the set of vortex generators having the larger chord. Blunt-lip configuration A was used in all tests presented herein where there were no generators or where the vortex generators having the smaller chord length were used. The definition of the configuration nomenclature is given in appendix B. (All symbols are defined in appendix A.) Centerbody performance bleed was ducted internally through the centerbody, passed through the four hollow support struts, and discharged overboard (fig. 2(b)). The bleed flow was throttled by choked butterfly valves at the exit of the struts.

The subsonic diffuser design was based on a quasi-one-dimensional flow analysis. The one-dimensional flow area used was based on an assumption of a linear variation in flow angle between the two surfaces. An attempt was made to design the subsonic diffuser for a linear variation of static pressure with axial distance and still maintain a short length. This resulted in an equivalent conical diffusion angle of 10° for the subsonic diffuser during Mach 2.5 operation. The area distribution within the diffuser is shown in figure 3. Two area distributions are shown: one for the Mach 2.5 centerbody, and the other for the Mach 2.0 centerbody.

Vortex generators were used on the cowl and centerbody to inhibit flow separation (figs. 2(a) and (b)). Details of the vortex generator design are shown in figure 4. Vortex generators, identified as set I, were designed such that the height or span of the airfoil was equal to about one-fourth of the Mach 2.5 inlet throat height. For set I the span of the airfoil on the cowl was equal to the span of the airfoil on the centerbody. The spacing of the set I vortex generators was such that it nearly satisfied the complete mixing criterion of reference 6. For vortex generator set II the span of the airfoil on the centerbody was different than that on the cowl and both were less than the span of set I. Spacing between the airfoils of set II was one-half that of set I. Airfoil spacing for the cowl and centerbody vortex generators of set II satisfied the complete mixing criterion of reference 6. Figure 4(a) gives the dimensions for the vortex generators on the cowl and the centerbody. Figure 4(b) shows the relative locations of vortex generator sets I and II with respect to the struts on both the cowl and the centerbody. The generators were configured such that they formed alternating converging and diverging flow passages on both the cowl and the centerbody. This resulted in two struts being located downstream of diverging flow passages, and two struts downstream of converging flow passages. The same number of generators were used on both the Mach 2.5 and 2.0 centerbodies. Since the spacing (D in fig. 4(a)) of the vortex generators on the centerbody was for the Mach 2.5 configuration, the same number of vortex generators resulted in a smaller spacing on the Mach 2.0 centerbody. The vortex generators were located at an axial distance x/R_c of 3.37 on each centerbody. The set II vortex generators installed in the inlet are shown in figure 5.

The inlet was also equipped with eight overboard bypass doors (fig. 2(b)) designed for high-frequency control studies. The doors were slotted plates which were hydraulically actuated. A detailed description of the bypass doors is presented in reference 5. The inlet was tested with and without an operating inlet bypass system. When bypass doors were not used, insert blanks replaced the bypass door assemblies so that smooth surfaces were maintained on the internal cowl from the cowl lip to the diffuser exit. A complete description of the inlet is given in reference 5.

Instrumentation

Steady-state instrumentation. - The static pressure variation throughout the inlet was determined from static pressure taps located along the top centerline of both the cowl and the centerbody. Additional static pressure taps were located 180° from the top centerline for both cowl and centerbody. The locations of the static pressure taps for the cowl and both the Mach 2.5 and Mach 2.0 centerbodies are given in table I.

The inlet flow was surveyed by total pressure probes at the throat and the throat exit, midway in the subsonic diffuser, and at the diffuser exit (fig. 2(b)). The boundary

layer on the cowl and centerbody at the throat was surveyed by the probes illustrated in figure 6(a). The details of the total pressure rakes at the mid-diffuser and throat exit locations for the two centerbodies are shown in figures 6(b) and (c). The rakes were circumferentially indexed to avoid mutual interference effects. All total pressures which were measured in regions of supersonic flow have not been corrected for shock losses. The values of pressure presented are therefore the indicated values behind the bow shock on the probe.

The details of the steady-state total and static pressure instrumentation at the compressor face are shown in figure 6(d). The overall diffuser exit area-weighted total pressure recovery was determined from rakes 1 to 12, which had six area-weighted tubes per rake. Rakes 1, 7, and 10 had three additional total pressure probes to better define the boundary layer on the cowl and centerbody at the diffuser exit. The angular location of the 12 rakes was adjusted for the presence of the four struts. This resulted in a 2.5° correction on eight of the 12 rakes adjacent to the struts. Wall static pressure measurements were made by using the 20 wall static pressure taps shown in figure 6(d).

Dynamic instrumentation. - In order to measure the fluctuating component of total pressure, a subminiature absolute pressure transducer was mounted in rake 1 shown in figure 6(d). The transducer was mounted in the rake such that a steady-state and a dynamic pressure measurement could be made simultaneously. The transducer was used to obtain the fluctuating component of pressure only. The installation of the dynamic pressure instrumentation is shown in figure 6(e). The resultant configuration provided a flat response to at least 1000 hertz, as shown in figure 6(f).

Pressure transducers were also located upstream and downstream of the vortex generators to measure static pressure fluctuations. Their installation is shown in figure 6(e). The upstream transducer was located about 2.54 cm ($x/R_c = 3.319$) ahead of the vortex generators. The downstream transducer was located 27.94 cm ($x/R_c = 3.908$) downstream of the upstream transducer (fig. 2(b)). These transducers were circumferentially located on the cowl 35° from the top centerline. The frequency response of the dynamic wall static pressure sensing system is shown in figure 6(g). There is no attenuation below about 1000 hertz, but there is amplification from about 100 to 1000 hertz. Inasmuch as the results presented herein are confined to an investigation of the frequency content, the amplification shown in the figure is acceptable.

The output signals of all pressure transducers passed through a second-order low-pass filter with a 1000-hertz corner frequency. The filtered fluctuating component of these pressure transducers was recorded on frequency-modulated magnetic tape.

Auto- and cross-correlations were obtained digitally by using the IBM Scientific Subroutine Package. The dynamic pressure data from the frequency-modulated tape were digitized at a rate of 2500 samples per second for 0.5 second. This resulted in a sample size of 1250 samples. The Nyquist frequency was 1250 hertz. Based on five

samples per cycle the frequency resolution was 500 hertz. The quantization error of the digitizing process was 0.015 rms noise-to-signal ratio. The maximum lag number for autocorrelation purposes was 167 based on a resolution of 15 hertz. The confidence level was 59 percent of a 30 percent error.

Test Procedure

A number of inlet operating conditions were investigated for each inlet configuration. Peak operation is defined as the minimum stable condition with the terminal shock at its most forward position in the inlet before unstart. Critical operation is defined as the terminal shock position at the inlet's geometric throat. Subcritical operation is defined as the range of operating conditions with the terminal shock located between the throat and the most forward position. Supercritical operation is hence defined as the range of operating conditions with the terminal shock downstream of the throat.

At the inlet design Mach number and contraction ratio and at zero angle of attack, a minimum centerbody bleed flow rate was determined that resulted in a maximum pressure recovery at critical inlet operation. This operating condition is referred to herein as the optimum centerbody bleed flow rate. (This procedure resulted in a very low centerbody bleed flow rate for this inlet.) Data were also taken for various overboard bypass flows (when the bypass system was operating) at the match compressor face corrected airflow required for the TF30-P-3. Data were taken at various compressor face corrected airflows by varying the choked plug area while keeping the bypass area at the original match point setting or with the overboard bypass system sealed. Results were obtained for values of centerbody bleed flow greater than optimum while the inlet was operating in a subcritical condition.

RESULTS AND DISCUSSION

Steady-State Performance

Area-weighted total pressure recovery and distortion. - The steady-state inlet performance is presented in figure 7. Results are presented for operation with and without vortex generators and for operation with both the design Mach 2.5 configuration and the off-design Mach 2.0 simulated collapsed configuration.

The improvement in performance attained by using set I vortex generators is shown in figure 7(a). The small differences in mass-flow ratio are due to the different centerbody bleed slot geometries used. As will be shown herein, the different slot geometries resulted in essentially identical nondimensional pressure profiles at the entrance to the

subsonic diffuser. The peak recovery increased from 0.889 without vortex generators to 0.904 when the vortex generators were used. As is well known, such an increase in performance is due to the improved mixing of the flow near the wall. The improved mixing also has a large effect on steady-state distortion. The distortion was reduced from 0.196 to 0.111 at peak operating conditions. As the terminal shock system was moved downstream, causing the inlet to operate supercritically, the distortion increased. The difference in distortion between operation with and without vortex generators, however, remained the same at all terminal shock positions.

The performance of the inlet with set II vortex generators installed is shown in figure 7(b). The performance is given for operation both with the overboard bypass operating and with the bypass sealed. Comparison of figures 7(a) and (b) shows that the peak recovery attained with the sealed bypass was nearly identical for operation with either set I or set II vortex generators (configurations Dccb and Accb, appendix B). The steady-state distortion was also essentially the same for critical operation with either set of vortex generators when the overboard bypass system was sealed.

As shown in figure 7(b) and discussed in reference 5, there is an additional loss in performance associated with the installation of an overboard bypass system. The peak total pressure recovery attained with bypass flow was identical to that attained without vortex generators or a bypass system. The gain in total pressure recovery associated with the use of vortex generators was therefore lost because of losses associated with the installation and operation of an overboard bypass flow system. In addition to the recovery losses associated with an operational overboard bypass system, distortion also increased. At peak operating conditions, with the overboard bypass system closed but with some bypass leakage flow, distortion increased to 13 percent. At critical operation, distortion further increased, to 15 percent. As the terminal shock moved supercritical, distortion remained fairly constant until the shock passed the generators (at a recovery of about 0.84). At this point it increased further. The distortion associated with the use of vortex generators is therefore less than that with no vortex generators but is adversely affected by the presence of an operational overboard bypass system.

The vortex generators on both the cowl and the centerbody were effective in improving the performance of the inlet, as shown in figure 7(c). Without generators the total pressure recovery for peak operation was 0.889 (figs. 7(a) and (b)). Adding generators on the centerbody (cb) increased the recovery while reducing the steady-state distortion. Adding generators to the cowl (ccb) then further reduced the distortion, as previously noted in figure 7(b), and increased the peak recovery. Similar improvements were noted for supercritical operation.

The performance of the simulated collapsed centerbody configuration for operation at Mach 2.0 and with set I and set II vortex generators is given in figure 7(d). The total pressure recovery at peak operation was slightly better with set I generators than with set II generators.

Static pressure distribution. - The distributions of static pressure on the cowl and centerbody for critical operating conditions are given in figure 8. The distributions shown are for operation with no vortex generators, with set I vortex generators, and with set II vortex generators. All data presented are for operation at Mach 2.5.

In figure 8(a) the distributions obtained with set I generators (configuration Dccb) are compared with distributions obtained with a configuration without generators (configuration A). The results were essentially the same for the two configurations on the cowl and the centerbody to the axial location of the vortex generators. At this location, x/R_c = 3.37, the vortex mixing action of the generators caused a sudden reduction in local static pressure on both the cowl and the centerbody. The reduction was more severe, however, on the cowl than on the centerbody. Downstream of the generator location and between x/R_c of 3.3 and 5.6, the measured diffusion was more rapid with generators than with no generators. This is a result of the vortex action causing a more uniform total pressure profile, which then permits a more efficient diffusion process.

The static pressure distributions that were obtained by using set II generators (configuration Accb) are compared with the distributions obtained without generators (configuration A) in figure 8(b). Data with overboard bypass flow and data with the bypass flow system sealed are presented. As expected the measured differences in static pressure distributions for these critical operating conditions are small upstream of the vortex generators. With operation using the set II generators the largest effect was again obtained on the centerbody at a x/R_c of about 3.37. Again there was a sudden decrease in static pressure across the vortex generators, followed by a more rapid subsonic diffusion process. The static distribution with generators was the same for operation with bypass flow and for operation with the bypass flow system sealed.

When the inlet was operated with generators on the centerbody only (configuration Acb), the static pressure distributions (not presented herein) obtained were similar to those obtained for operation with generators on both walls. The vortex action with generators on the centerbody only was not as strong as with generators on each surface. As a result the gains in performance were not as great and the decrease in static pressure, characteristic of operation with vortex generators, was not as great at the generator location (x/R_c = 3.37). With vortex generators on each surface the reenergizing of the low-energy flow near the wall permitted a more rapid diffusion downstream of about x/R_c = 3.4 without encountering separation problems, as shown in figure 8(b).

Diffuser total pressure profiles. - The total pressure profiles at the throat on both the centerbody and the cowl, at the throat exit, at the mid-diffuser, and at the diffuser exit are shown in figures 9 to 13. All profiles shown in the figures are for critical terminal shock position. The total pressure profiles at the diffuser exit are for only the top quadrant of the four quadrants defined by the location of the four struts. The pressure profiles in the other three quadrants were virtually identical to those presented because the inlet was at zero angle of attack.

The profiles for configuration A (without vortex generators) are given in figure 9. The profiles at the throat (figs. 9(a) and (b)) showed an apparently well-defined viscous layer 5 to 10 percent of the passage height in thickness on both surfaces. As is discussed in reference 5 the shape of the centerbody total pressure profile (at a ratio of distance from surface to rake height d/H = 0.05) was partially attributable to an expansion wave emanating from the leading edge of the bleed slot on the centerbody. The recovery in the free stream was high, with the recovery slightly higher on the cowl than on the centerbody. At the exit of the throat the viscous layer had begun to grow, and losses began to appear on the cowl. At the mid-diffuser location the viscous layer had become very thick, and incipient separation was indicated on the centerbody. The profiles at the diffuser exit showed thick viscous layers on both the cowl and the centerbody (fig. 9(e)). Separation was indicated at each midquadrant profile (rake 1) on the centerbody. The rake positions adjacent to the struts showed that the flow near the centerbody was not separated but was near separation. The flow on the cowl was also near separation, as evidenced by the pressure distribution in the regions near the wall (rake 1).

The total pressure profiles obtained with configuration Dccb (set I vortex generators) are shown in figure 10. For critical operation the pressure profiles at the throat and the throat exit were essentially identical to those presented for configuration A (fig. 9). The flow in the diffuser had been successfully improved by the addition of vortex generators, as shown in figure 10(d). The flow was no longer near separation, as evidenced by the substantial pressure gradient near the centerbody wall. The pressure farther from the wall was not extremely uniform, however, because the vortex action of the generators did not have sufficient time to decay. The profiles at the diffuser exit are shown in figure 10(e). The high-recovery regions shown in the profiles obtained without generators had been mixed with the flow near the walls to prevent separation. The resultant profiles were more uniform near the walls.

The recovery profiles are shown in figure 11 for configuration Accb (set II vortex generators) and critical operation at Mach 2.5. The throat and throat exit profiles were similar to those of the configurations presented in figures 9 and 10. The mid-diffuser profile was flat except near the centerbody. Comparison of figures 10(d) and 11(d) indicated that the vortex action of the set II generators was more successful in energizing this flow and reducing flow distortion. The total pressure profiles at the exit of the diffuser (fig. 11(e)) were nearly the same as those for configuration Dccb (fig. 10(e)). The profiles obtained with the set II generators were somewhat more uniform than those associated with set I generators. This implies a better mixing of the high-energy air with the low-energy air and suggests that the vortex action of the set I generators had not sufficiently decayed.

The performance of simulated collapsed configuration Dccb (set I vortex generators) operating at Mach 2.0 is shown in figure 12. For critical operation the pressure profiles at the throat (figs. 12(a) and (b)) showed a very good recovery except near the walls.

The apparent viscous layer was again 5 to 10 percent of the passage height on both the cowl and the centerbody. At the throat exit the wall viscous layer had grown somewhat, but the overall profile across the passage was acceptable and showed high recoveries. The pressure profile at the mid-diffuser measuring station was more uniform and showed higher recoveries at Mach 2.0 operation than at design (Mach 2.5) operation.

The pressure profiles obtained with simulated collapsed configuration Accb (set II vortex generators) are shown in figure 13 for Mach 2.0 critical operation. The results at the throat and the throat exit are similar to those presented in figure 12. The flow distortion at the mid-diffuser, however, was larger with configuration Accb than with configuration Dccb. Large radial variations in recovery at the diffuser exit are shown in figure 13(e). On the other hand, there were almost no circumferential variations. The vortex generators were successful in preventing separation on both walls, but with the larger throat height they did not mix all the high-energy core near the center of the channel with the flow near each wall. Nevertheless, the average recovery was high and there were no separation problems. The set II vortex generators, therefore, had the better performance at the design condition but were not superior to the set I vortex generators at off-design operation.

The importance of having generators on both the cowl and the centerbody to reduce distortion is shown in figure 14. The profiles shown in this figure are for a configuration with generators on the centerbody only. Comparison of the profiles with those previously presented (fig. 11(e)) indicated that the vortex action induced by the centerbody vortex generators did not result in a radial readjustment of the flow nor did it affect the flow near the cowl. The nearly separated flow shown in figure 9(e) was still present, and a very nonuniform pressure profile existed at the diffuser exit (fig. 14).

Diffuser exit total pressure contours. - The diffuser exit total pressure contours are shown in figure 15 for critical operation for configurations A, Dccb, Acb, and Accb. The contours are based on spline fits of the pressure measurements obtained from the 12 rakes shown in figure 6(d) and do not account for the presence of the struts. The positions of the struts are shown in the figure. As has already been discussed, when no generators were used, large radial gradients in total pressure occurred and the flow separated on the centerbody. This is reflected in the contour presented in figure 15(a) as the large low-recovery region on the centerbody. The contours are radial with little or no circumferential component. When generators were added to the cowl and the centerbody, the pressure contours became more uniform, as shown in figures 15(b) and (c). Comparison of the contours obtained with vortex generator sets I and II showed that the vortex action induced by the set II generators decayed more.

The pressure contour obtained with generators located only on the centerbody (configuration Acb, fig. 15(d)) clearly indicates the success of the generators in making the pressure profiles more uniform on the centerbody. The region of high-pressure gradient near the cowl remained and was not affected by the generators. As was shown from the

results of figure 14, vortex generators are therefore necessary on both surfaces for uniform diffuser exit pressure profiles.

The pressure contours for simulated collapsed configuration Accb operating at Mach 2.0 are shown in figure 15(e). As was shown from the radial plots of pressure profile (fig. 12(e)), the contours are basically radial with regions of high-pressure recovery located near midspan. There is no indication of separation on either surface.

Correlations of Fluctuating Pressures

In addition to the steady-state performance characteristics of the vortex generators, their effects on the time-variant flow characteristics in the diffuser can be significant. The vortex action of the generators alters the turbulent mixing characteristics of the flow in the near-wall region and the time-varying distortion characteristics at the diffuser exit. Information about these effects induced by the vortex generators is necessary for the designer to properly account for the presence of the generators in the subsonic diffuser design. The fluctuating component of the wall static pressure was therefore recorded upstream and downstream of the vortex generators. In addition, a total pressure was recorded at the diffuser exit. These three pressures were used in the investigation. The fluctuating component of the wall static pressure measured upstream of the vortex generator location is called the "upstream pressure." The fluctuating component of the wall static pressure measured downstream of the vortex generator location is called the "downstream pressure." The third pressure considered is the fluctuating component of the total pressure measured at the diffuser exit, called the "diffuser exit pressure." The relative locations at which these pressures were recorded are shown in figures 2(c), 6(d), and 6(e). The characteristics of these three fluctuating pressures were investigated by examining the auto- and cross-correlations.

Autocorrelations of fluctuating pressures. - The autocorrelations of the fluctuating component of the static pressure measured upstream and downstream of the vortex generators and the diffuser exit total pressure are shown in figure 16. Data are presented for critical operation both with and without the vortex generators installed. The autocorrelation coefficients decayed rapidly and showed no periodic frequency for any of the three measurements for the two inlet configurations presented. Data obtained for operation at other terminal shock positions were similar to the data presented herein.

Correlation function coefficient. - The transmission path of flow disturbance between the vortex generator location and the diffuser exit was investigated by studying the cross-correlations of the upstream, downstream, and diffuser exit dynamic pressures. The results are presented in figure 17 in terms of the correlation function coefficient (CFC). The correlation function coefficient is a normalized cross-covariance function of two waveforms and is a measure of their similarity as a function of the time shift

between the waveforms (ref. 7). Therefore, for a pure advection process, the magnitude of the CFC should have a peak value of 1.0. This peak value should occur at a lag time determined by the flow velocity and the transmission path length. Deviations from a peak value of 1.0 imply an influence of waveforms originating from other sources. Acoustical propagation and turbulent mixing are two common examples of such sources. Each of the three possible correlation function coefficients are presented: (1) correlation of the upstream wall dynamic static pressure with the downstream wall dynamic static pressure, (2) correlation of the upstream wall dynamic static pressure with the diffuser exit dynamic total pressure, and (3) correlation of the downstream wall dynamic static pressure with the diffuser exit dynamic total pressure.

Correlation of the wall dynamic static pressures upstream and downstream of the vortex generator location are given in figure 17(a) for critical inlet operation. The CFC's for critical operation are similar both with (configuration Accb) and without (configuration A) generators installed. There is no indication of any transmission path time other than the very short time associated with either the advection of the pressure signal by the flow or an acoustical propagation between the two wall static pressure taps. CFC magnitudes less than about 0.2 are not believed to be significant, and no relevance is attached to any associated peaks The transmission time based on local velocities is expected to be of the order of 0.001 second, whereas the transmission time based on acoustic propagation is expected to be about 0.0005 second. The magnitude of the CFC can be attenuated by many possible sources of turbulent mixing between the two measurement stations. The peak magnitude of the CFC occurred near zero time and was significantly less than 1. This implies that substantial mixing had occurred between the two measuring stations. The presence of the vortex generators had no apparent effect on the peak magnitude of the CFC, as shown in figure 17(a).

The CFC's of the wall dynamic static pressures with the dynamic diffuser exit total pressure are given in figures 17(b) and (c) for critical operation. The data presented are for operation both with and without generators installed. For the separation distances of the measuring stations, the expected transmission times associated with flow advection and acoustic propagation were about 0.005 and 0.002 second, respectively. There was no indication of any significant transmission times near these values. For operation without vortex generators the peak CFC again occurred near zero time. For operation with vortex generators the vortex action resulted in sufficient mixing that this near-zero-time peak was absent. Therefore, all upstream effects were completely wiped out when vortex generators were used.

When the inlet was configured without vortex generators, the CFC's indicated a very short transmission time, of the order of 0.001 second or less. The complete absence of transmission times associated with flow advection implies that the flow may be acting like a solid body transmitter. As was discussed earlier, the flow separated on the centerbody and was near separation on the cowl when vortex generators were not used

(figs. 9(a) and 10(a)). The time-unsteady separation characteristics were therefore such that the separation region was fluctuating and the conditions at the diffuser exit were almost immediately influenced by the upstream flow fluctuations.

SUMMARY OF RESULTS

An experimental investigation was made to determine the effects of two sets of vortex generators on the steady-state total pressure recovery and distortion at the subsonic diffuser exit of an axisymmetric mixed-compression supersonic inlet. The time-varying flow characteristics associated with the vortex generators were also investigated. The two sets of vortex generators were similar in design and differed primarily in chord and aspect ratio. The inlet was designed for Mach 2.5 operation. The external compression was provided by a bicone centerbody having half-angles of 12.5° and 18.5°. Forty-five percent of the supersonic area contraction occurred internally.

Data were obtained at Mach 2.0 for a collapsed version of the inlet centerbody and at the inlet design condition of Mach 2.5. The Reynolds number at the design Mach number was 8.2 million per meter. The following results were obtained:

1. With no vortex generators, the flow separated in the subsonic diffuser. The separation adversely affected the area-weighted total pressure recovery and distortion at the diffuser exit. Both sets of vortex generators tested were successful in eliminating separation. Total pressure recovery was increased and steady-state distortion was reduced. The vortex generators with the smaller chord and aspect ratio were the most efficient.

2. The signal transmission paths associated with the dynamics of the flow at the vortex generators and near the diffuser exit were studied. When the inlet was operated without vortex generators, the diffuser flow was separated. The correlation function coefficient indicated that the flow at the diffuser exit was immediately influenced by the dynamics of the flow near the vortex generator location. With vortex generators, the vortex action of the generators wiped out all effect of the upstream pressure on the diffuser exit pressure. The correlation function coefficient indicated no single source of influence at the diffuser exit. The fluctuating pressure signal at the diffuser exit was therefore influenced by other signals, which were beyond the scope of this investigation.

Lewis Research Center,
National Aeronautics and Space Administration,
Cleveland, Ohio, November 12, 1974,
505-04.

APPENDIX A

SYMBOLS

A	flow area, sq m
A_c	capture area, 0.7073 sq m
$C_x(\tau)$	autocovariance function of sample random process x(t) at time t and lag time τ (hence, $C_x(0)$ is evaluated at lag time $\tau = 0$), $C_x(\tau) = \frac{1}{N-r}\sum_{n=1}^{N-r}(x_n - \bar{x})(x_{n+r} - \bar{x})$ where lag number $r = N\tau/(\text{Total sample time}) = 0, 1, 2, \ldots, m < N$ and N is number of digitized samples, m is maximum lag number, and x is sample random process
$C_{xy}(\tau)$	cross covariance function between sample random processes x(t) and y(t) at time t and lag time τ
$C_y(\tau)$	autocovariance function of sample random process y(t) at time t and lag time τ (hence, $C_y(0)$ is evaluated at lag time $\tau = 0$), $C_y(\tau) = \frac{1}{N-r}\sum_{n=1}^{N-r}(y_n - \bar{y})(y_{n+r} - \bar{y})$
d	distance from surface, m
H	annulus height at local diffuser station, m
h	height of total pressure rake, m
M	Mach number
m_2/m_0	mass-flow ratio
P	total pressure, N/sq m
p	static pressure, N/sq m
R_c	inlet capture radius, 0.4745 m
x	axial location, m
$\rho_x(\tau)$	autocorrelation coefficient, $C_x(\tau)/C_x(0)$
$\rho_{xy}(\tau)$	correlation function coefficient, $C_{xy}(\tau)/\sqrt{C_x(0)C_y(0)}$ at time τ

φ circumferential rake position, deg

Subscripts:

max maximum

min minimum

x local

y local

0 free stream

2 diffuser exit station

Superscript:

– area-weighted average

APPENDIX B

CONFIGURATION NOMENCLATURE

The first capital letter in the configuration nomenclature (such as Accb) refers to the centerbody bleed slot. The centerbody bleed configurations are shown in figures 2(d) and (e). The sharp-lip configuration is designated by D and the blunt-lip configuration by A. The use of vortex generators is indicated by either cb or ccb. If generators are used on the centerbody only, the designation cb is used. If generators are used on both the centerbody and the cowl, the designation ccb is used. If neither designation is used, vortex generators were not used on either surface.

REFERENCES

1. Mitchell, Glenn A.; and Davis, Ronald W.: Performance of Centerbody Vortex Generators in an Axisymmetric Mixed Compression Inlet at Mach Number of 2.0 to 3.0. NASA TN D-4675, 1968.

2. Mitchell, Glenn A.: Experimental Investigation of the Performance of Vortex Generators Mounted in the Supersonic Portion of a Mixed-Compression Inlet. NASA TM X-2405, 1971.

3. Calogeras, James E.; Burstadt, Paul L.; and Coltrin, Robert E.: Instantaneous and Dynamic Analysis of Supersonic Inlet-Engine Compatibility. AIAA Paper 71-667, June 1971.

4. Wasserbauer, Joseph F.; Shaw, Robert J.; and Neumann, Harvey E.: Minimizing Boundary Layer Bleed for a Mixed Compression Inlet. NASA TM X-71461, 1973.

5. Wasserbauer, Joseph F.; Shaw, Robert J.; and Neumann, Harvey E.: Design of a Very-Low-Bleed Mach 2.5 Mixed-Compression Inlet with 45 Percent Internal Contraction. NASA TM X-3135, 1975.

6. Taylor, H. D.: Application of Vortex Generator Mixing Principles to Diffusers. Rept. R-15064-5, United Aircraft Corp., 1948.

7. Bendat, Julius S.; and Piersol, Allan G.: Random Data; Analysis and Measurement Procedures. Wiley-Interscience, pp. 71-74.

ORIGINAL PAGE IS
OF POOR QUALITY

TABLE I. - INLET COORDINATES

(a) Cowl

x/R	r/R	x/R	r/R
2.0148	1.0000	4.0148	0.9745
2° Internal		4.0683	.9746
cowl angle		4.1218	.9748
2.2117	1.0069	4.1754	.9749
2.2455	1.0079	4.2289	.9751
2.2761	1.0084	4.2824	.9753
2.3058	1.0086	4.3360	.9756
2.3348	1.0086	4.3895	.9759
2.3631	1.0082	4.4430	.9761
2.3908	1.0075	4.4965	.9763
2.4180	1.0065	4.5501	.9765
2.4447	1.0053	4.6036	.9768
2.4710	1.0038	4.6571	.9770
2.4971	1.0021	4.7107	.9771
2.5381	0.9993	4.7642	.9774
2.5786	.9967	4.8177	.9776
2.6187	.9944	4.8713	.9779
2.6584	.9924	4.9242	.9781
2.6978	.9906	4.9783	.9783
2.7369	.9889	5.0319	.9785
2.7760	.9872	5.0854	.9787
2.7836	.9869	5.1389	.9790
2.8371	.9850	5.1924	.9792
2.8906	.9831	5.2460	.9794
2.9442	.9813	5.2995	.9796
2.9977	.9794	5.3530	.9798
3.0512	.9778	5.4066	.9800
3.1048	.9763	5.4601	.9802
3.1583	.9754	5.5136	.9805
3.2118	.9748	5.5672	.9807
3.2653	.9745	5.6207	.9808
3.3189	.9743	5.6742	.9809
3.9612	.9743	5.8209	.9809

(b) Mach 2.5 centerbody

x/R	r/R	x/R	r/R
0	0	3.8542	0.6777
12.5° Conical section		3.9077	.6709
1.0001	0.2217	3.9612	.6638
18.5° Conical section		4.0148	.6554
2.3749	0.6817	4.0683	.6466
2.4408	.7036	4.1218	.6363
2.5068	.7251	4.1754	.6255
2.5733	.7463	4.2289	.6137
2.5831	.7494	4.2824	.6016
Bleed slot		4.3360	.5893
2.6883	0.7547	4.3895	.5768
2.7283	.7526	4.4430	.5645
2.7836	.7497	4.4965	.5521
2.8371	.7469	4.5501	.5397
2.8906	.7441	4.6036	.5273
2.9442	.7413	4.6571	.5149
2.9977	.7384	4.7107	.5025
3.0512	.7356	4.7642	.4902
3.1048	.7328	4.8177	.4778
3.1583	.7300	4.8713	.4654
3.2118	.7272	4.9248	.4530
3.2653	.7242	4.9783	.4406
3.3189	.7211	5.0319	.4282
3.3724	.7179	5.0854	.4159
3.4259	.7146	5.1389	.4035
3.4795	.7110	5.1924	.3911
3.5330	.7072	5.2460	.3787
3.5865	.7032	5.2995	.3661
3.6401	.6990	5.3530	.3538
3.6936	.6942	5.4066	.3413
3.7471	.6892	5.4601	.3354
3.8007	.6836	5.8209	.3354

(c) Mach 2.0 centerbody

x/R	r/R	x/R	r/R
0	0	3.8542	0.5541
12.5° Conical section		3.9077	.5470
1.0001	0.2217	3.9612	.5397
14.5° Conical section		4.0148	.5323
2.3509	0.5711	4.0683	.5248
2.4053	.5851	4.1218	.5174
2.4597	.5991	4.1754	.5100
2.5144	.6128	4.2289	.5026
2.5695	.6264	4.2824	.4951
2.6160	.6377	4.3360	.4877
Bleed slot		4.3895	.4803
2.7222	0.6429	4.4430	.4728
2.7836	.6397	4.4965	.4654
2.8371	.6369	4.5501	.4580
2.8906	.6341	4.6036	.4505
2.9442	.6313	4.6571	.4431
2.9977	.6285	4.7107	.4357
3.0512	.6257	4.7642	.4282
3.1048	.6229	4.8177	.4208
3.1583	.6200	4.8713	.4134
3.2118	.6171	4.9248	.4060
3.2653	.6135	4.9783	.3985
3.3189	.6097	5.0319	.3911
3.3724	.6055	5.0854	.3837
3.4259	.6011	5.1389	.3762
3.4795	.5963	5.1924	.3688
3.5330	.5912	5.2460	.3614
3.5865	.5858	5.2995	.3539
3.6401	.5803	5.3530	.3461
3.6936	.5741	5.4066	.3386
3.7471	.5677	5.4601	.3354
3.8007	.5610	5.8209	.3354

(a) Installation in 10- by 10-Foot Supersonic Wind Tunnel.

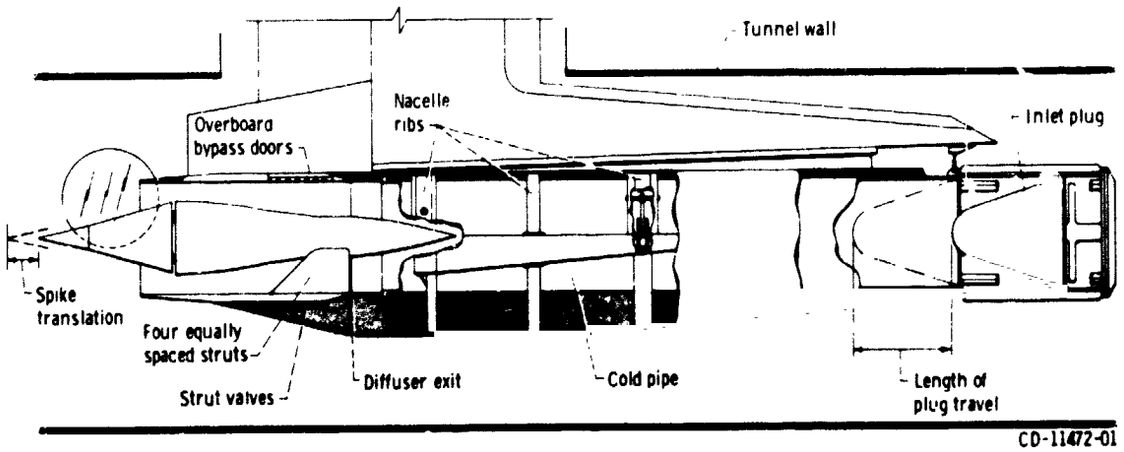

(b) Nacelle cutaway illustrating cold-pipe installation.

Figure 1. - Inlet model.

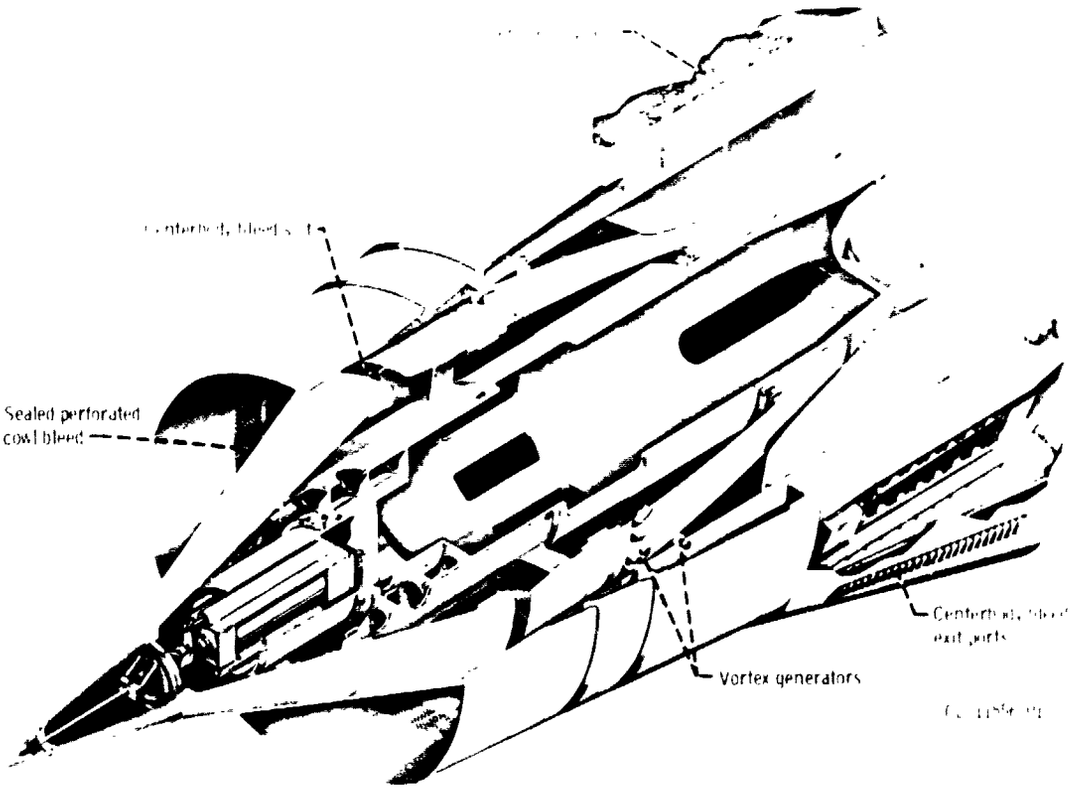

(a) Isometric view.

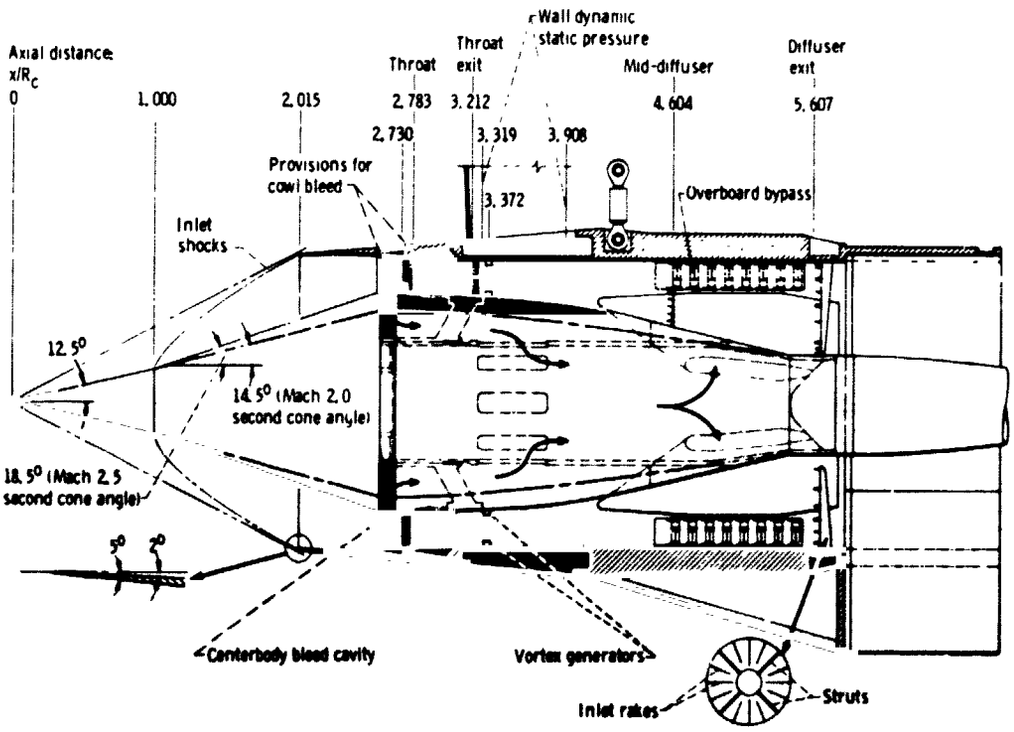

(b) Cross section and diffuser instrumentation.

CD-11473-01

Figure 2. - Details of inlet model.

ORIGINAL PAGE IS
OF POOR QUALITY

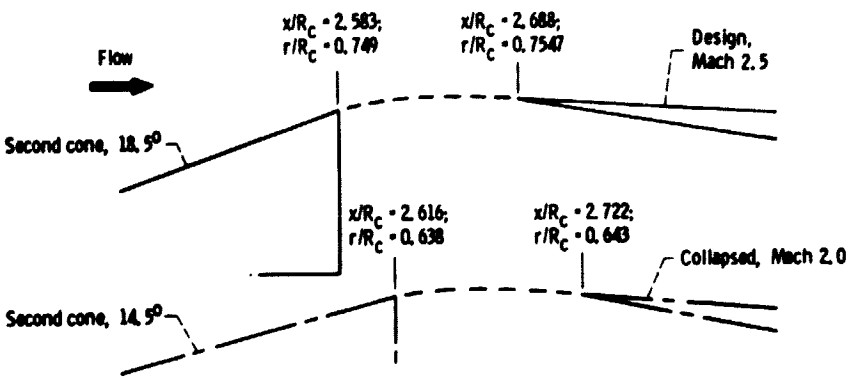

(c) Configuration D; sharp lip, flush slot.

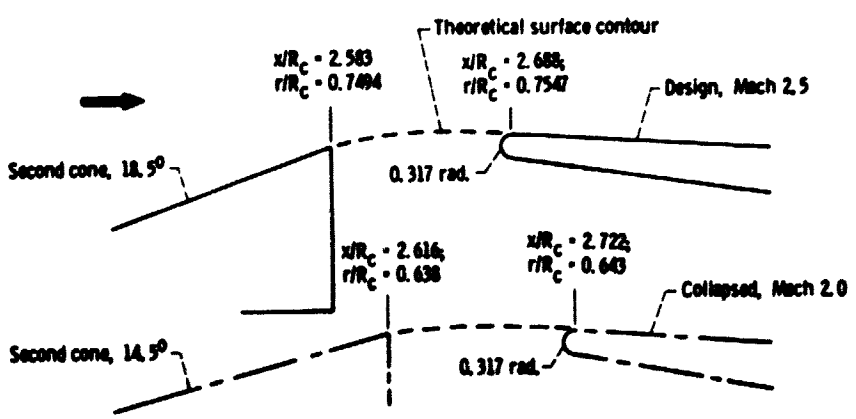

(d) Configuration A; blunt lip, flush slot.

Figure 2. - Concluded.

ORIGINAL PAGE IS
OF POOR QUALITY

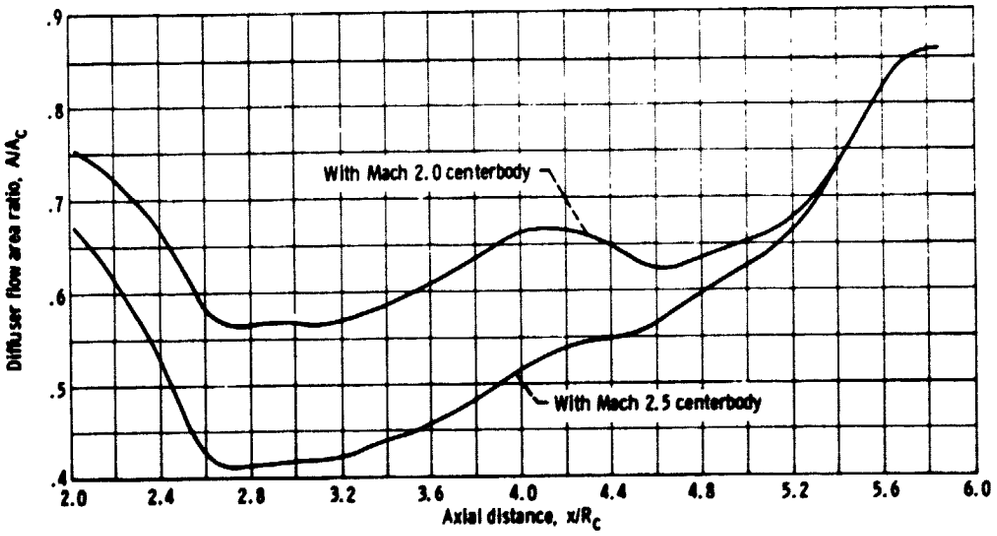

Figure 3. - Area variation within diffuser.

Set	Location	Dimension, cm				
		A	B	C	D	E
I	Cowl	0.305	5.044	2.54	9.682	0.051
	Centerbody	.305	5.044	2.54	9.723	.051
II	Cowl	0.229	3.048	1.52	4.841	0.030
	Centerbody	.305	4.064	2.03	4.862	.041

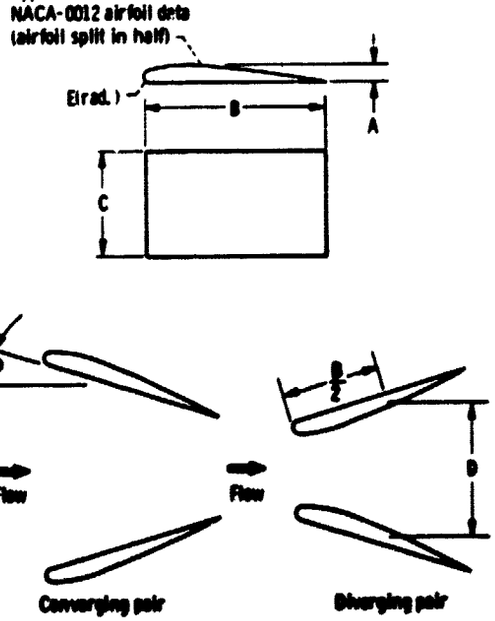

(a) Vortex generator detail.

Figure 4. - Vortex generator design.

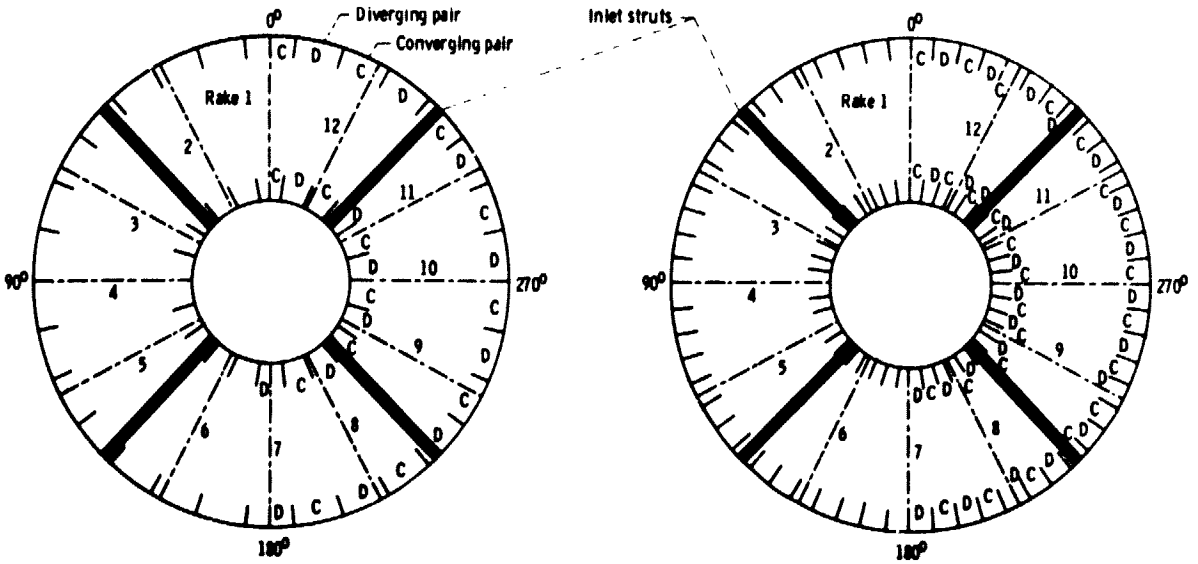

(b) Vortex generator installation, view looking downstream. (Vortex generators on centerbody only are denoted by cb; vortex generators on cowl and centerbody are denoted by ccb.)

Figure 4. - Concluded.

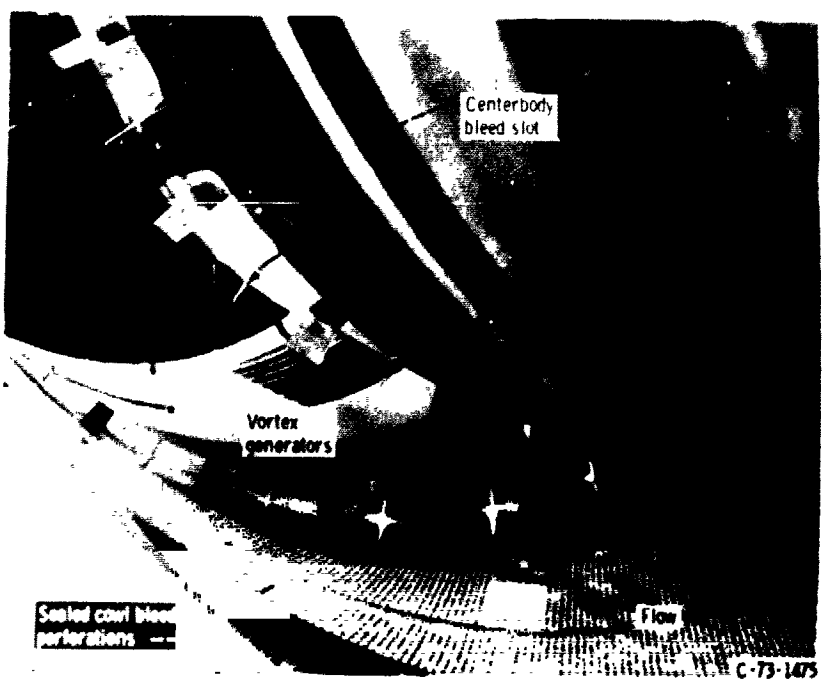

Figure 5. - Vortex generators installed in inlet.

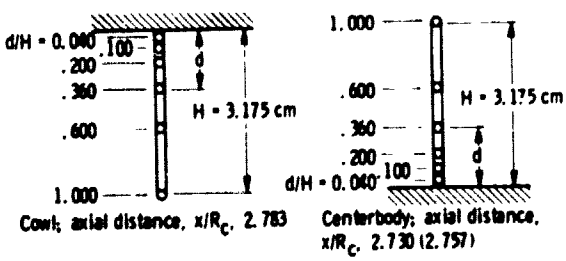

Cowl; axial distance, x/R_c, 2.783

Centerbody; axial distance, x/R_c, 2.730 (2.757)

(a) Cowl and centerbody throat boundary layer total pressure rakes. Circumferential position, φ, 10°. (Dimension for Mach 2.0 centerbody is given in parentheses.)

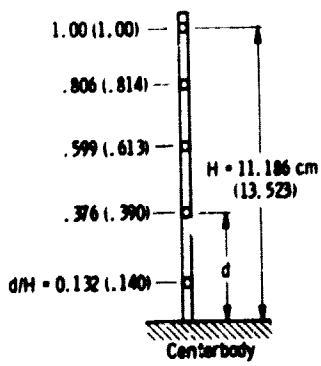

(b) Mid-diffuser total pressure rake. Circumferential position, φ, 0°; axial distance, x/R_c, 4.604. (Dimensions for Mach 2.0 centerbody are given in parentheses.

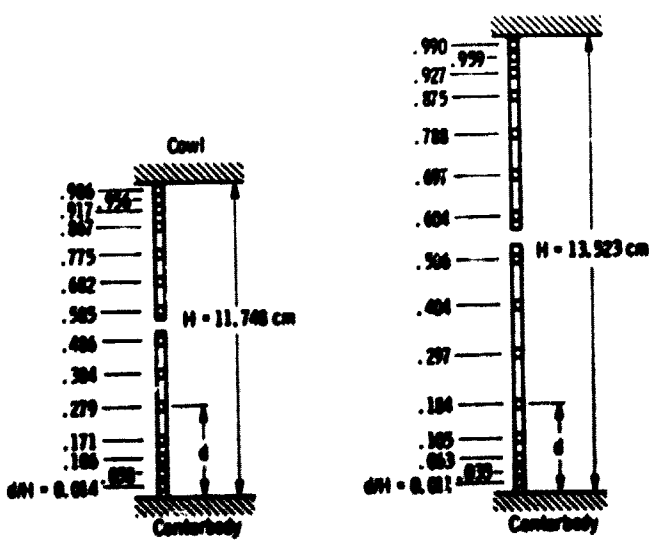

Mach 2.5 centerbody

Mach 2.0 centerbody

(c) Throat exit total pressure rakes. Circumferential position, φ, 350°; axial distance, x/R_c, 3.212.

Figure 6. - Inlet pressure instrumentation.

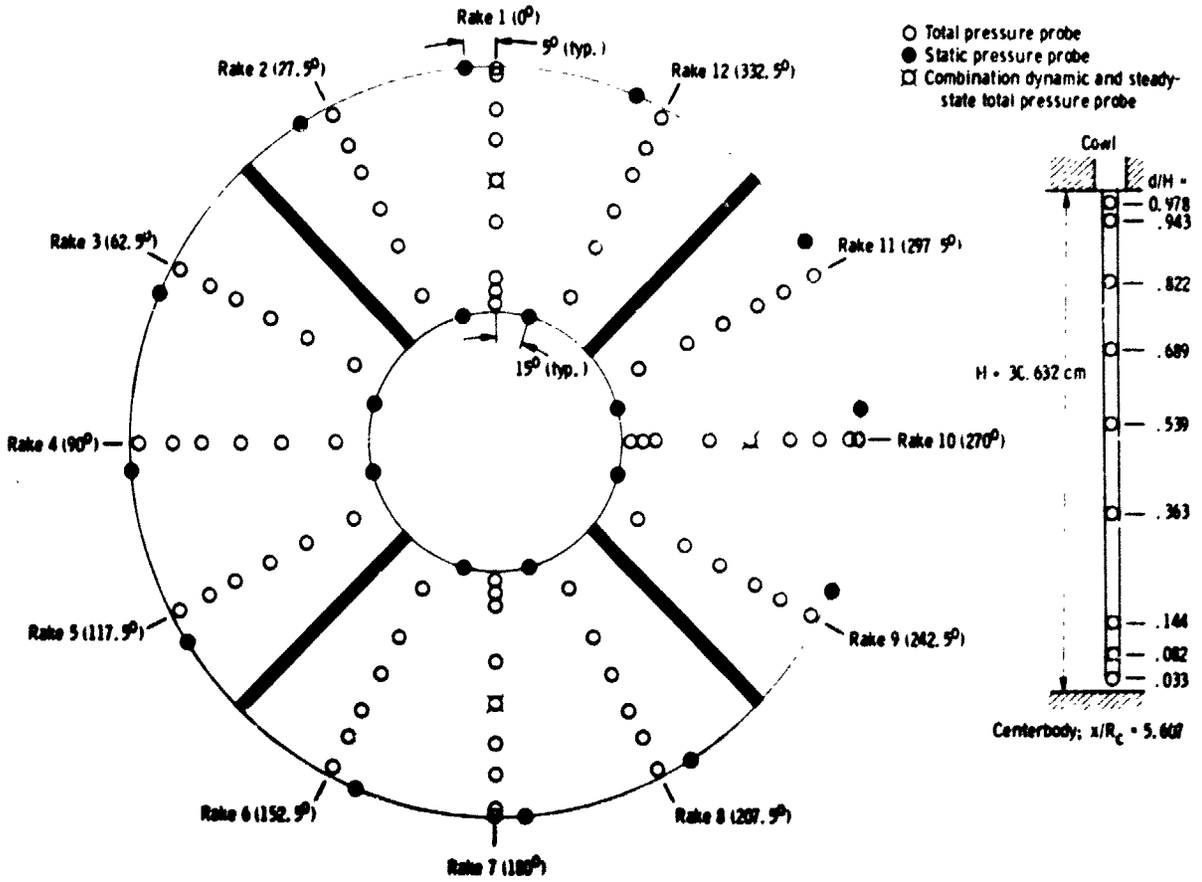

(d) Diffuser exit steady-state pressure instrumentation, at station 2 (looking downstream).

Figure 6. - Continued.

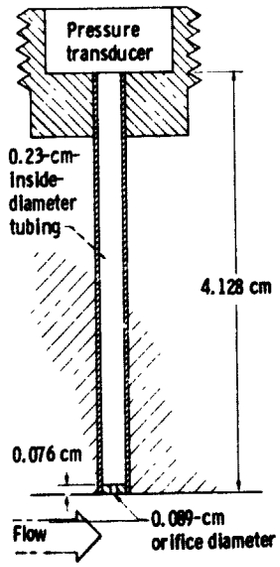

Dynamic static pressure transducer installation in cowl wall at x/R_c = 3.319 and 3.908 and $\varphi = 35^0$ from model top centerline

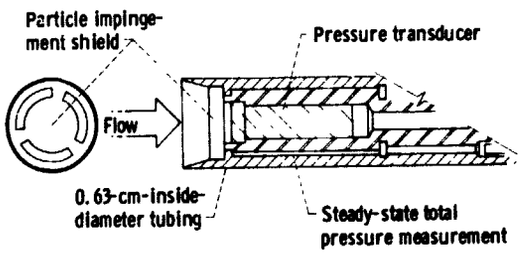

Combination steady-state and dynamic total pressure probe tip used at subsonic diffuser exit

(e) Dynamic instrumentation.

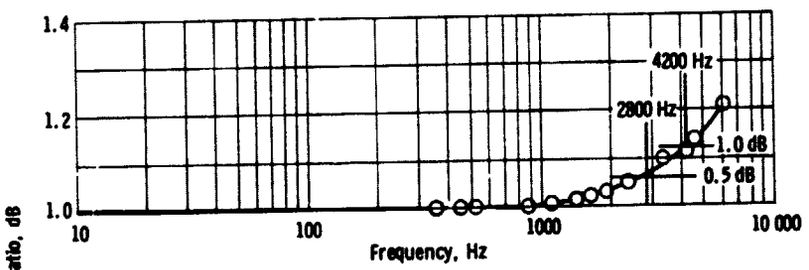

(f) Frequency response of dynamic total-pressure-sensing system.

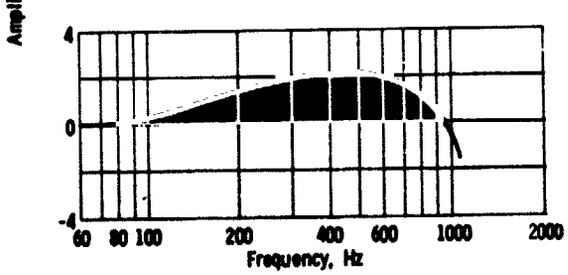

(g) Frequency response of dynamic static-pressure-sensing system.

Figure 6. - Concluded.

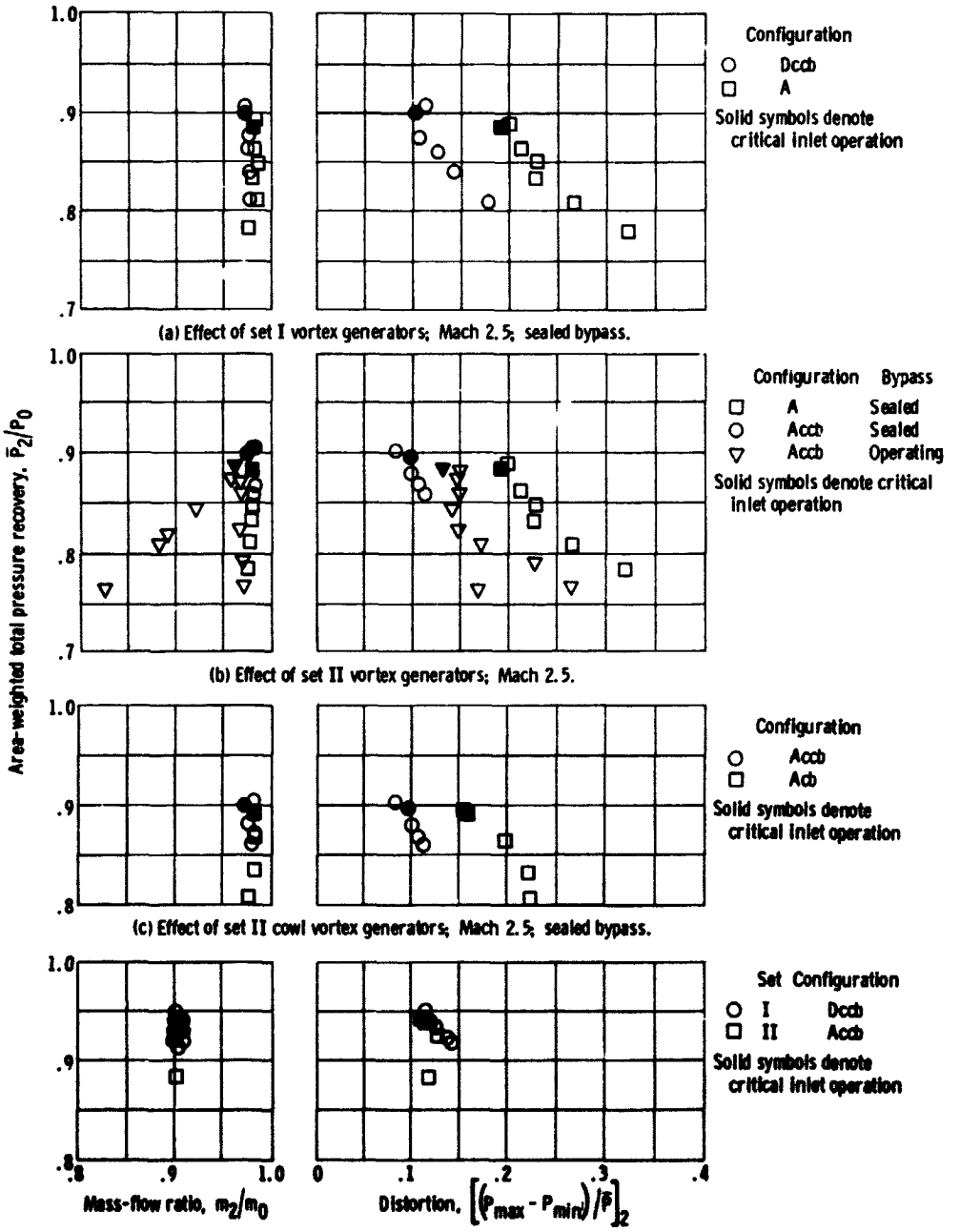

Figure 7. - Steady-state inlet performance.

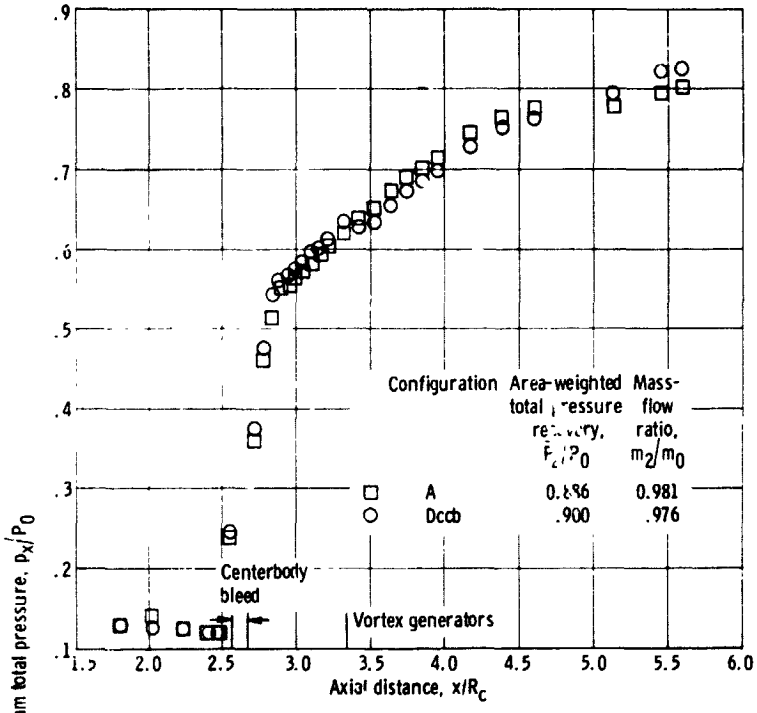

(a-1) Centerbody.

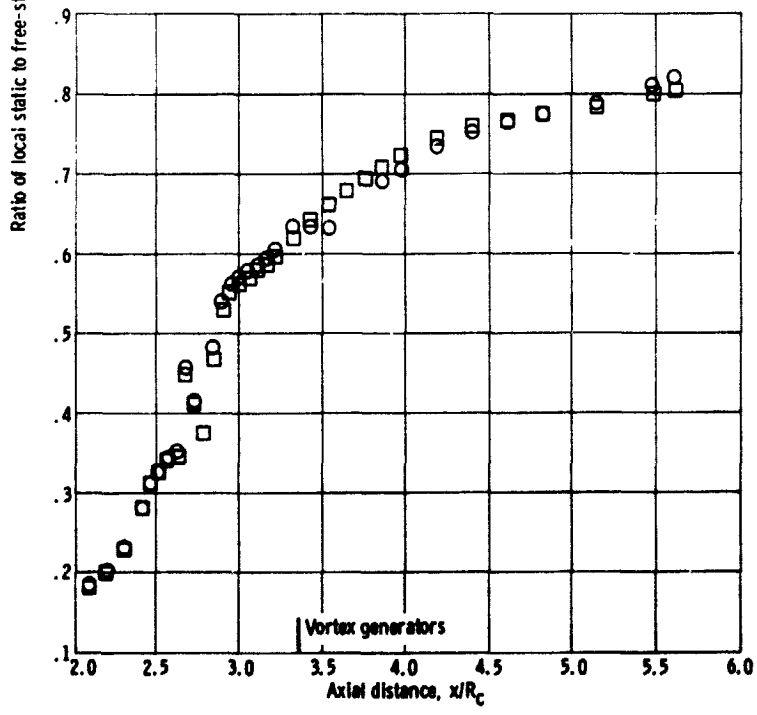

(a-2) Cowl.

(a) Effect of set I vortex generators.

Figure 8. - Static pressure distributions for critical inlet operation. Sealed bypass; free-stream Mach number, M_0, 2.5.

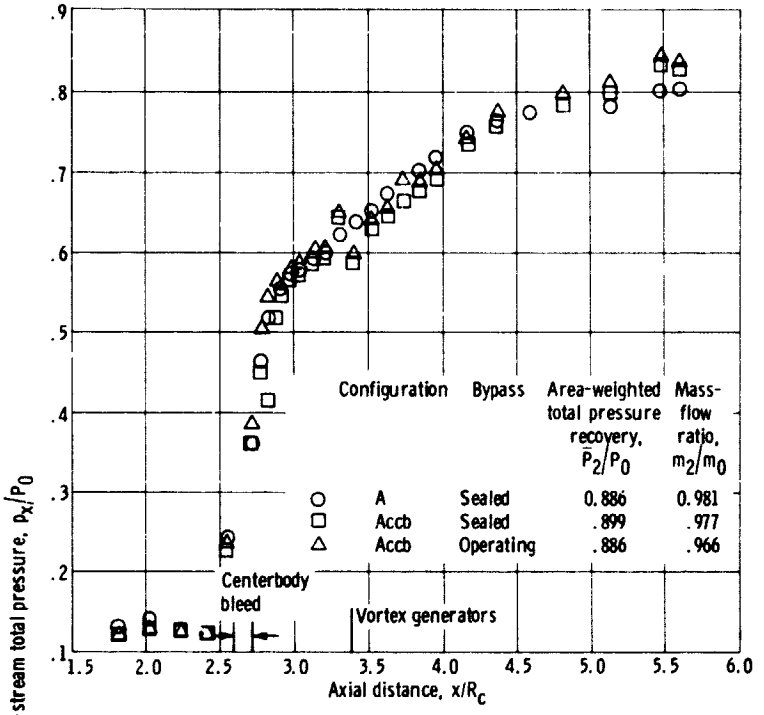

(b-1) Centerbody.

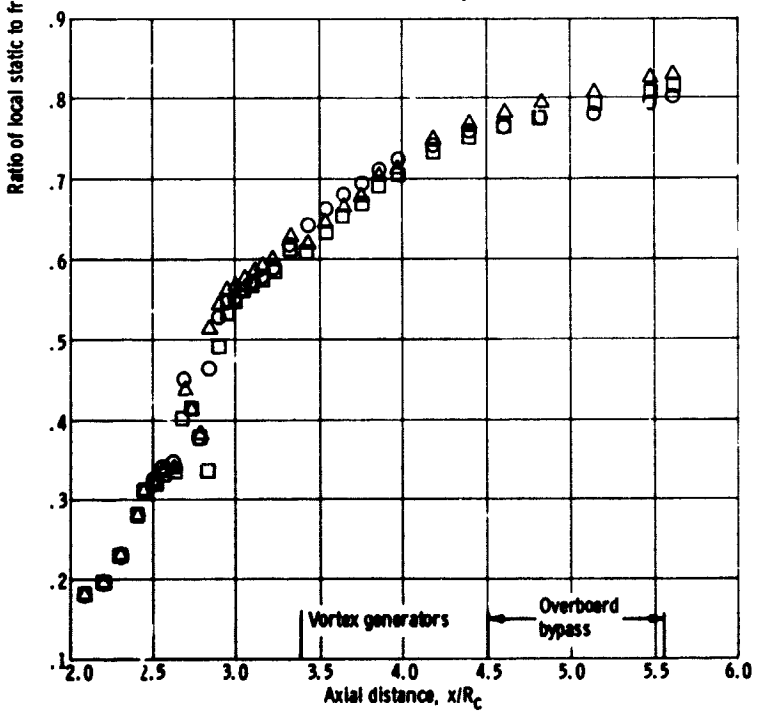

(b-2) Cowl.

(b) Effect of set II vortex generators.

Figure 8. - Concluded.

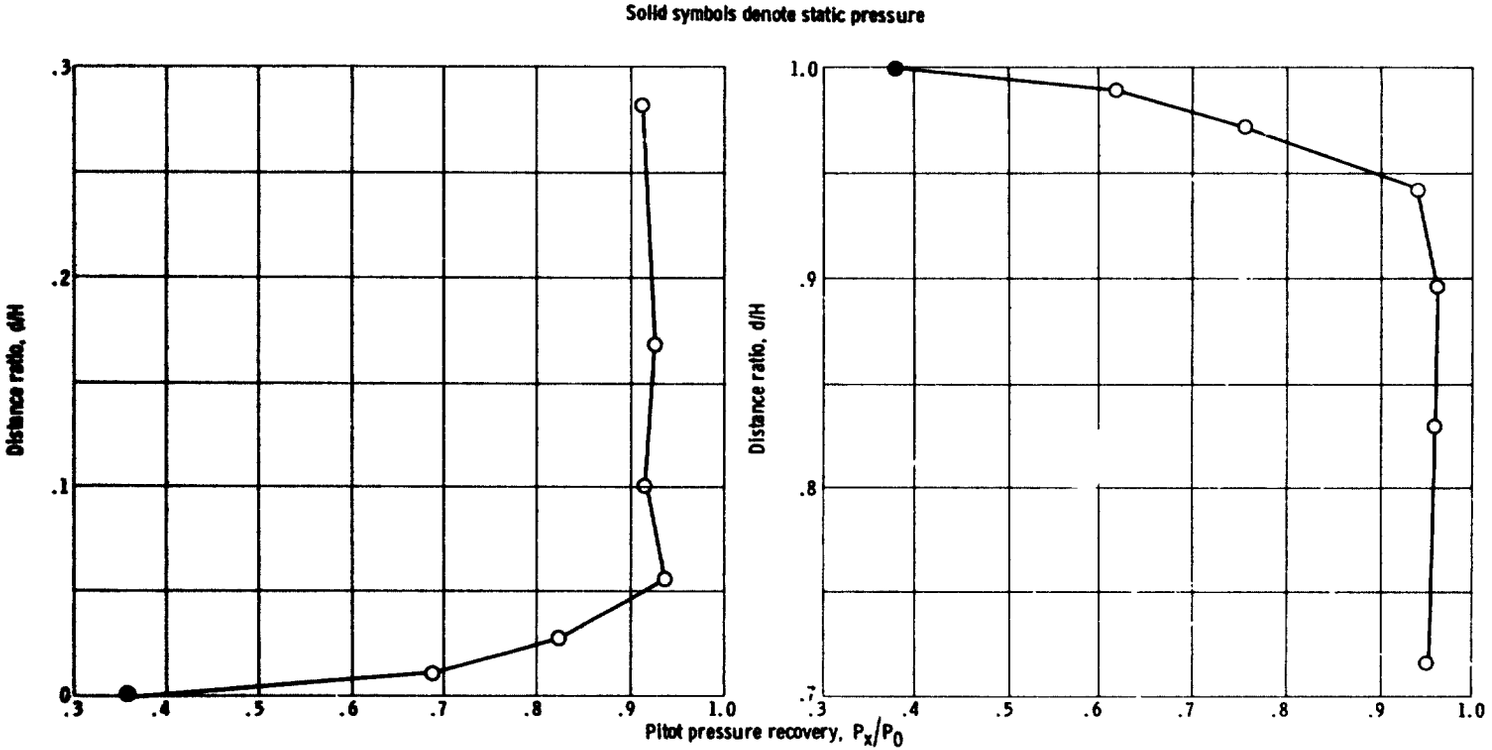

(a) Centerbody throat boundary layer rake.

(b) Cowl throat boundary layer rake.

Figure 9. - Total pressure profiles without vortex generators; configuration A; sealed bypass; area-weighted total pressure recovery, $\bar{P}_2/P_0$, 0.886; mass-flow ratio, m_2/m_0, 0.981; free-stream Mach number, M_0, 2.5; critical inlet operation.

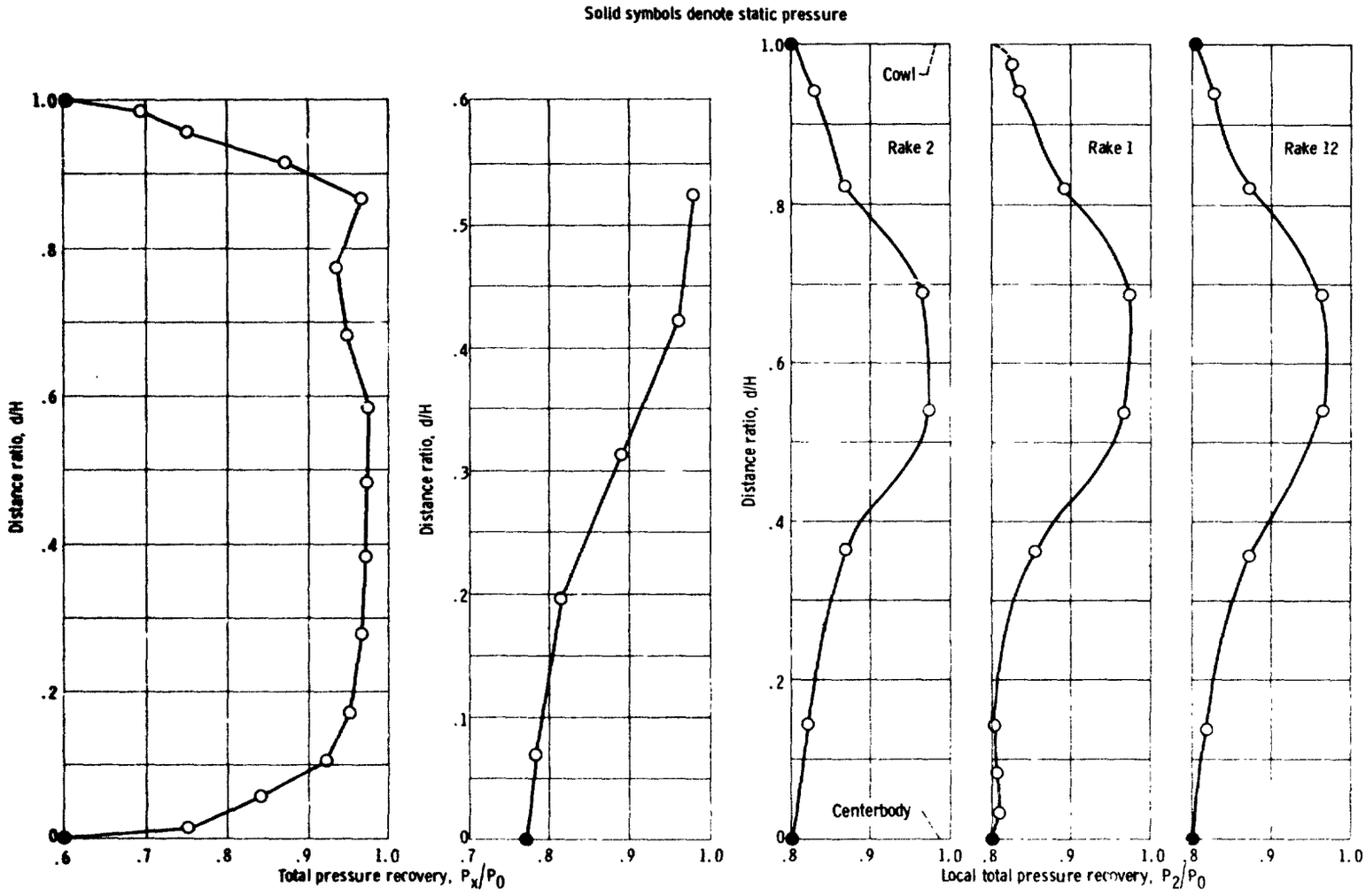

(c) Throat exit rakes. (d) Mid-diffuser rake. (e) Diffuser exit rakes, top quadrant.

Figure 9. - Concluded.

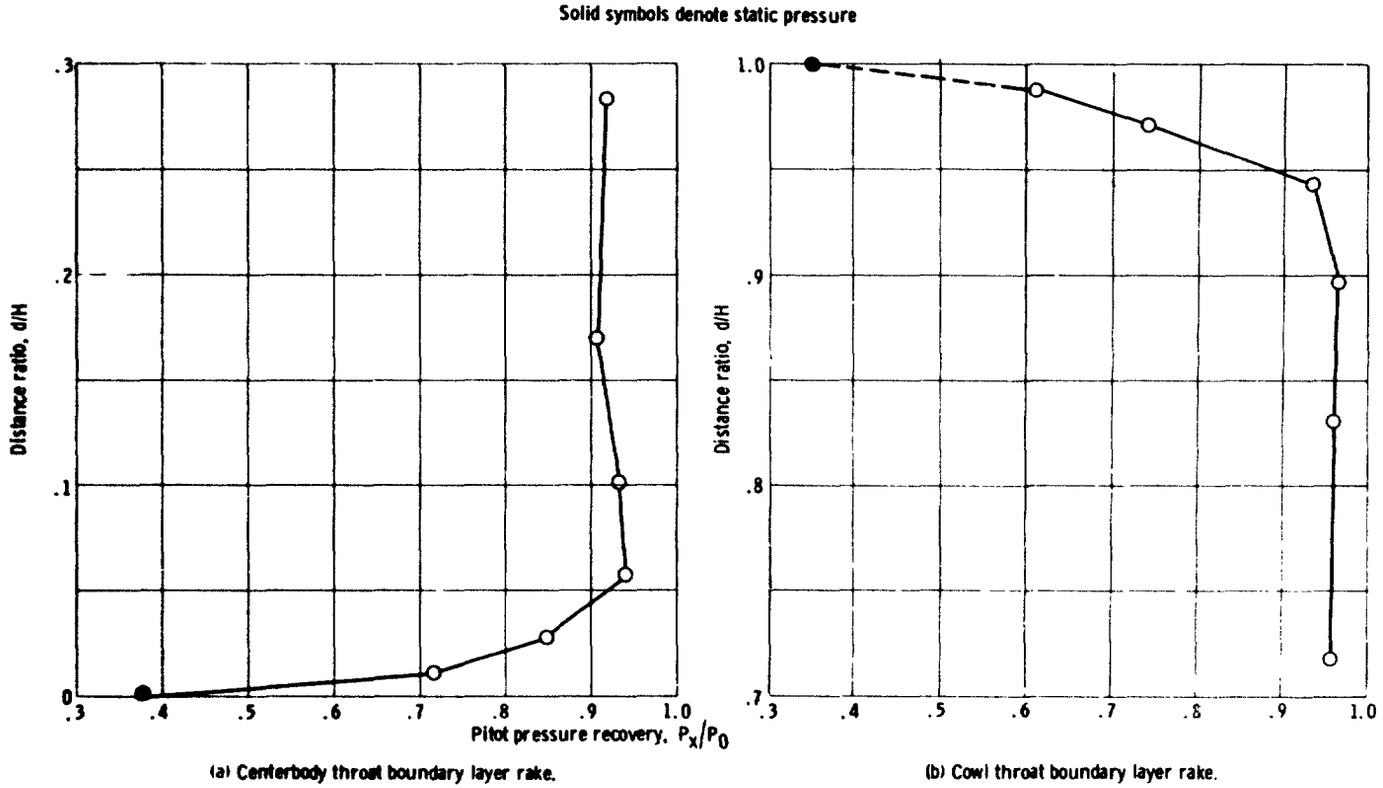

(a) Centerbody throat boundary layer rake.

(b) Cowl throat boundary layer rake.

Figure 10. - Total pressure profiles with set I vortex generators; configuration Dccb; sealed bypass; area-weighted total pressure recovery, $\bar{P}_2/P_0$, 0.900; mass-flow ratio, m_2/m_0, 0.976; free-stream Mach number, M_0, 2.5; critical inlet operation.

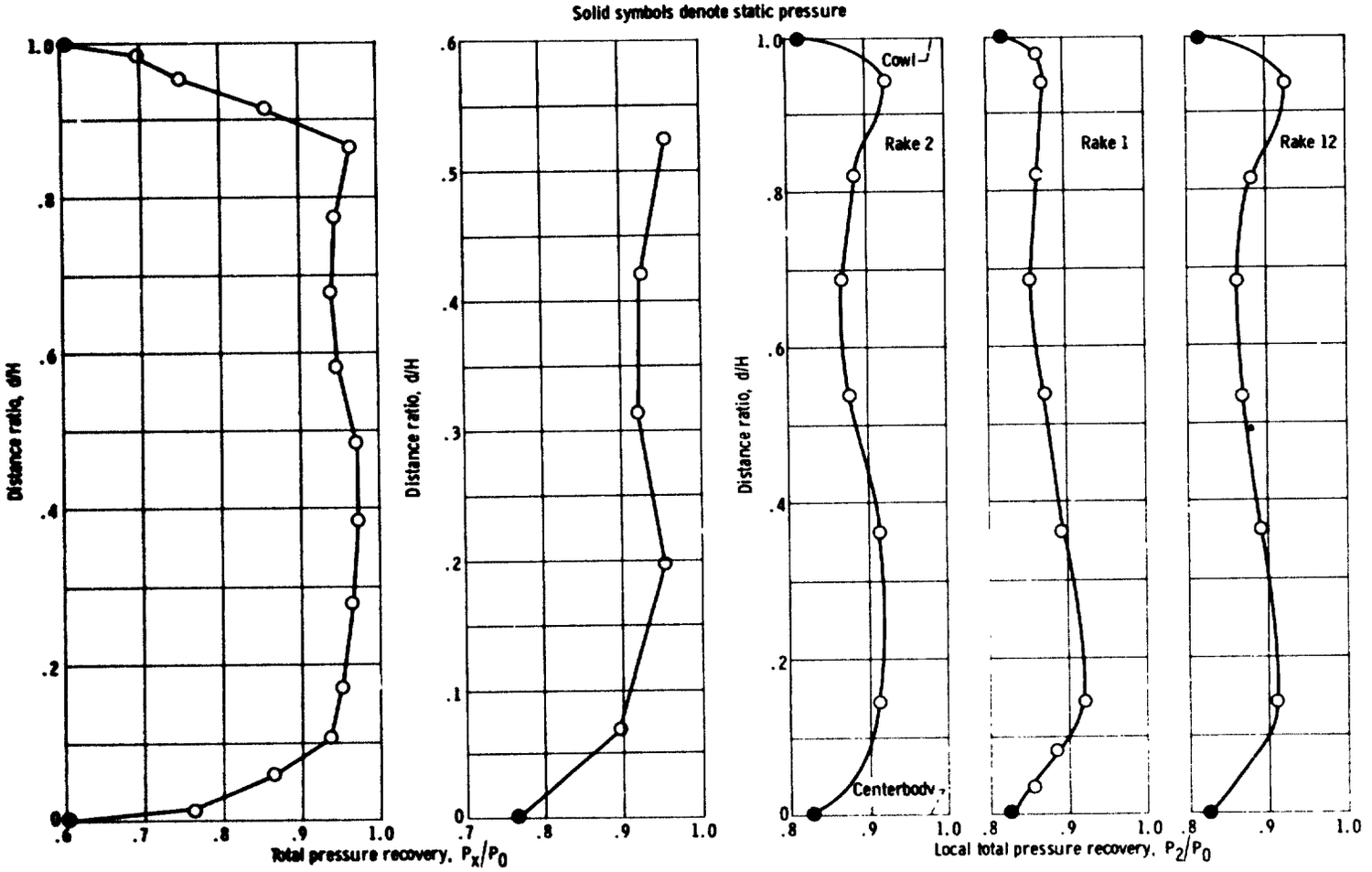

(c) Throat exit rakes.

(d) Mid-diffuser rake.

(e) Diffuser exit rakes, top quadrant.

Figure 10. - Concluded.

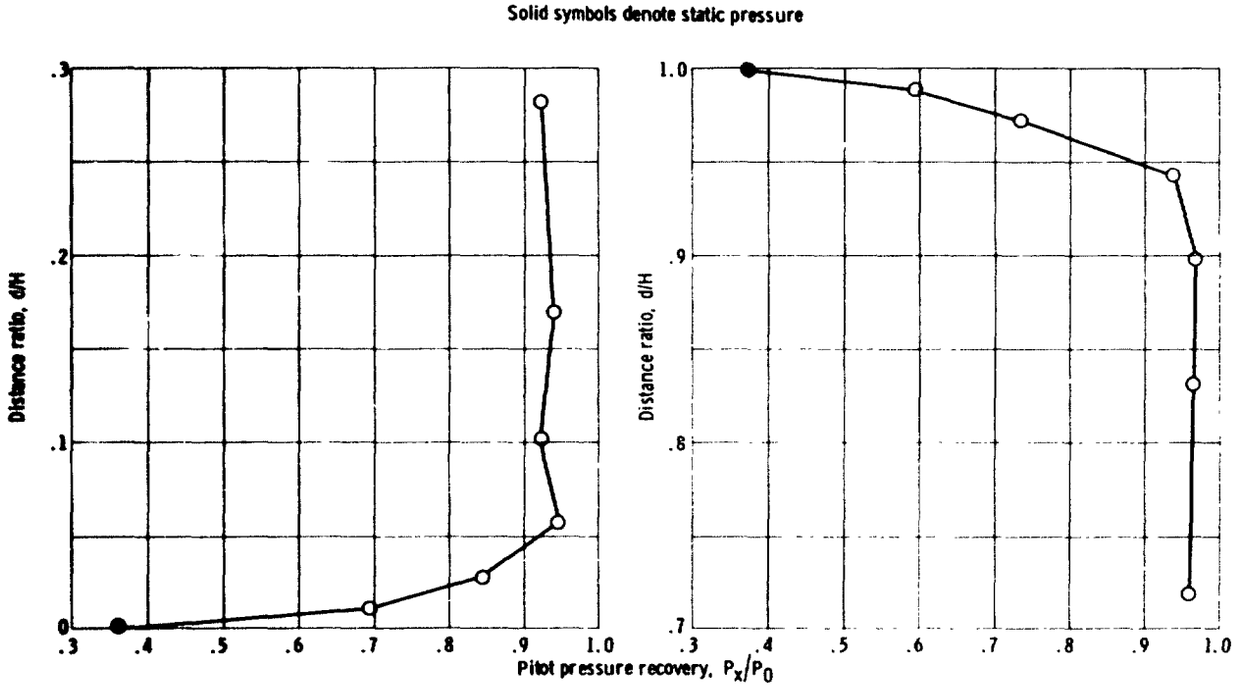

(a) Centerbody throat boundary layer rake.

(b) Cowl throat boundary layer rake.

Figure 11. - Total pressure profiles with set II vortex generators; configuration Accb; sealed bypass; area-weighted total pressure recovery, $\bar{P}_2/P_0$, 0.899; mass-flow ratio, m_2/m_0, 0.977; free-stream Mach number, M_0, 2.5; critical inlet operation.

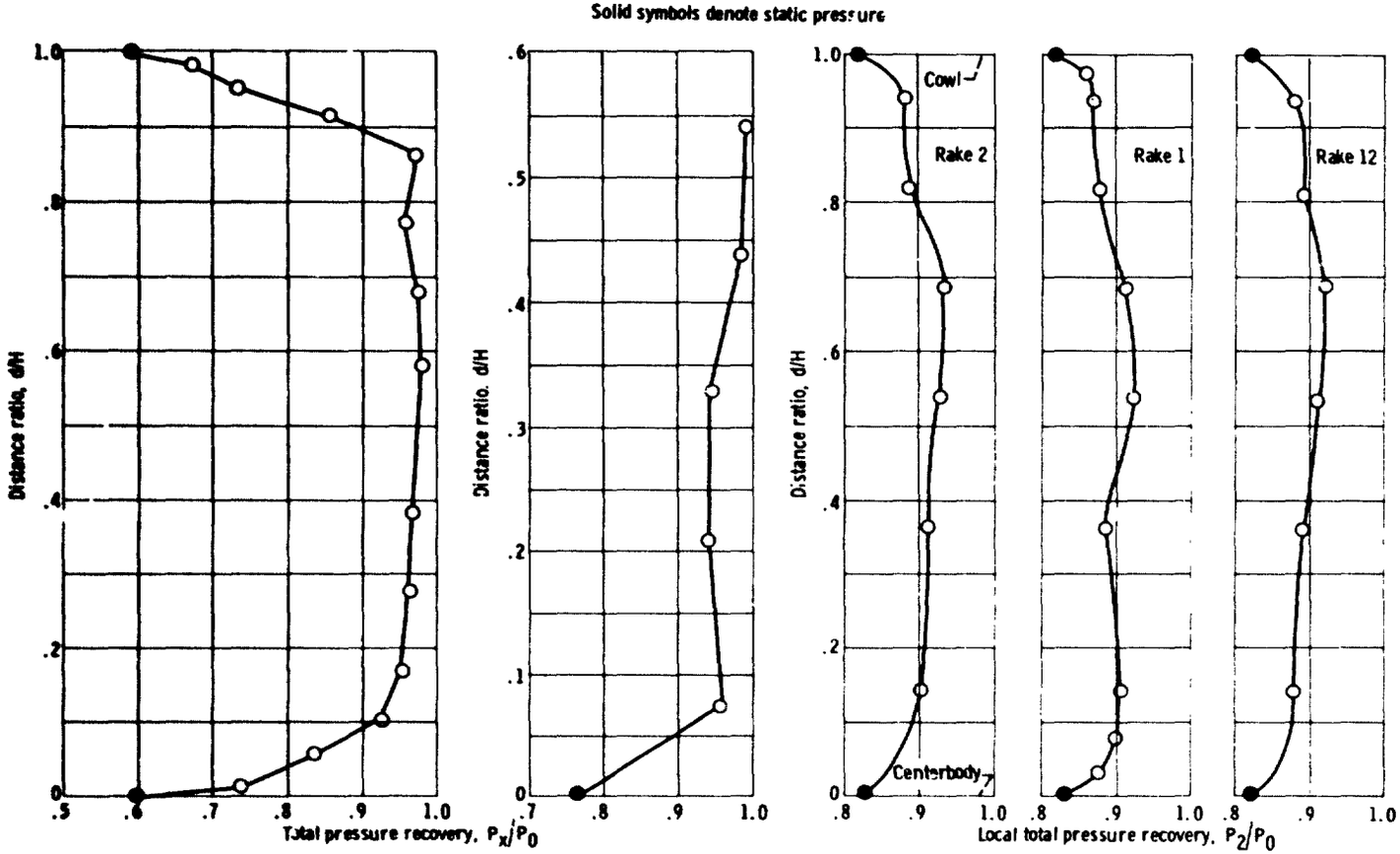

(c) Throat exit rakes. (d) Mid-diffuser rake. (e) Diffuser exit rakes, top quadrant.

Figure 11. - Concluded.

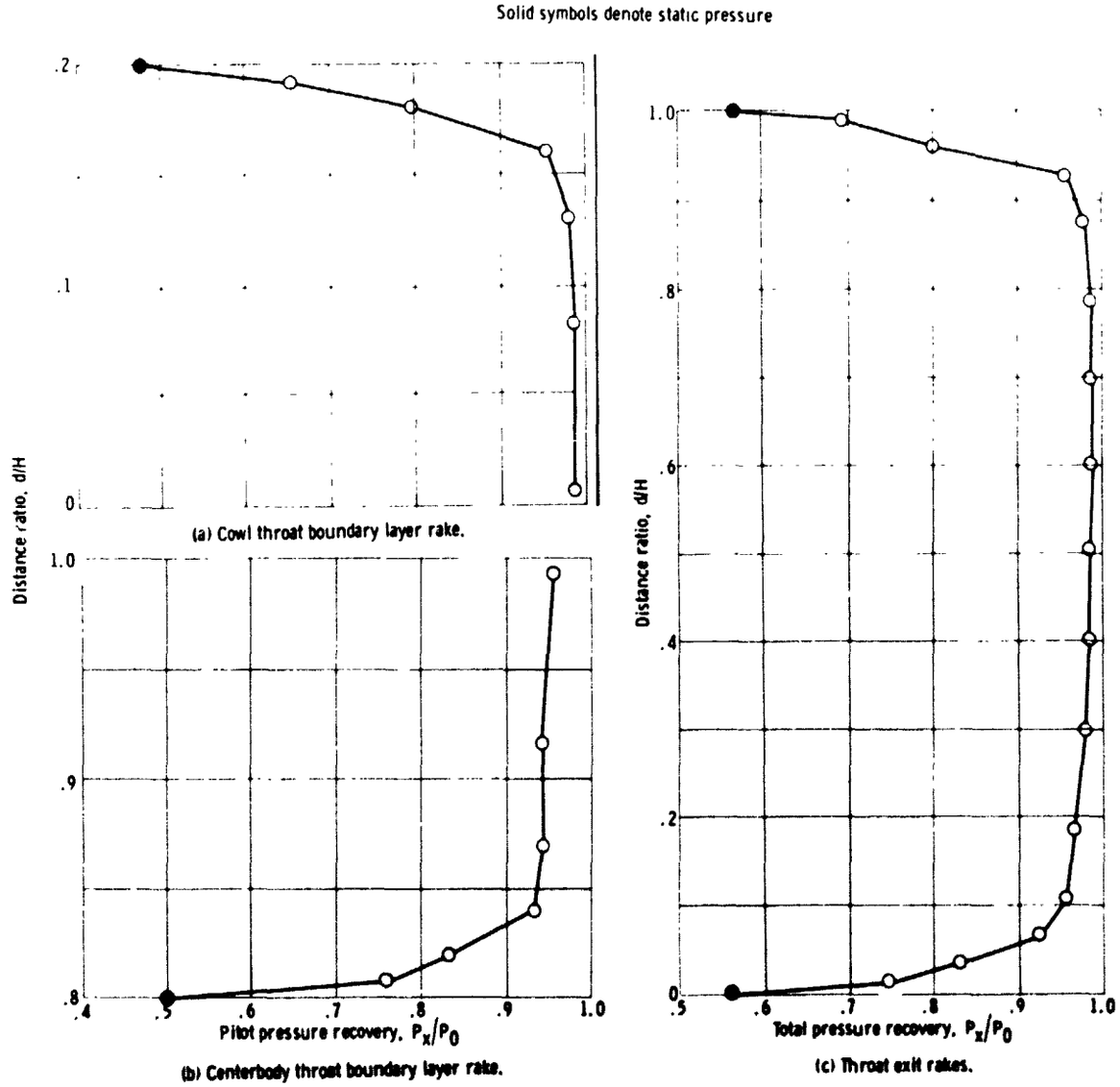

Figure 12. - Total pressure profiles with set I vortex generators; configuration Dccb, sealed bypass; area-weighted total pressure recovery, $\bar{P}_2/P_0$, 0.935; mass-flow ratio, m_2/m_0, 0.908; free-stream Mach number, M_0, 2.0; critical inlet operation.

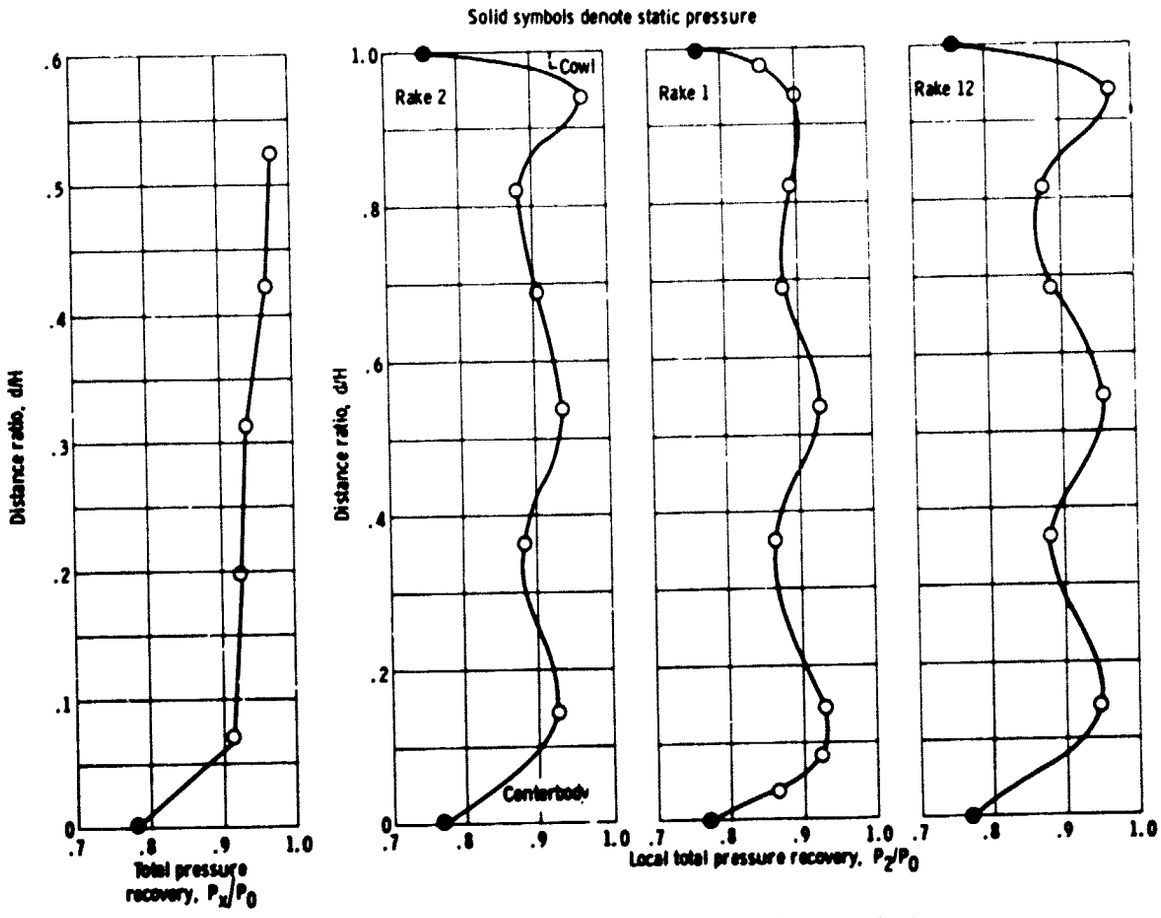

(d) Mid-diffuser rakes.

(e) Diffuser exit rakes, top quadrant.

Figure 12. - Concluded.

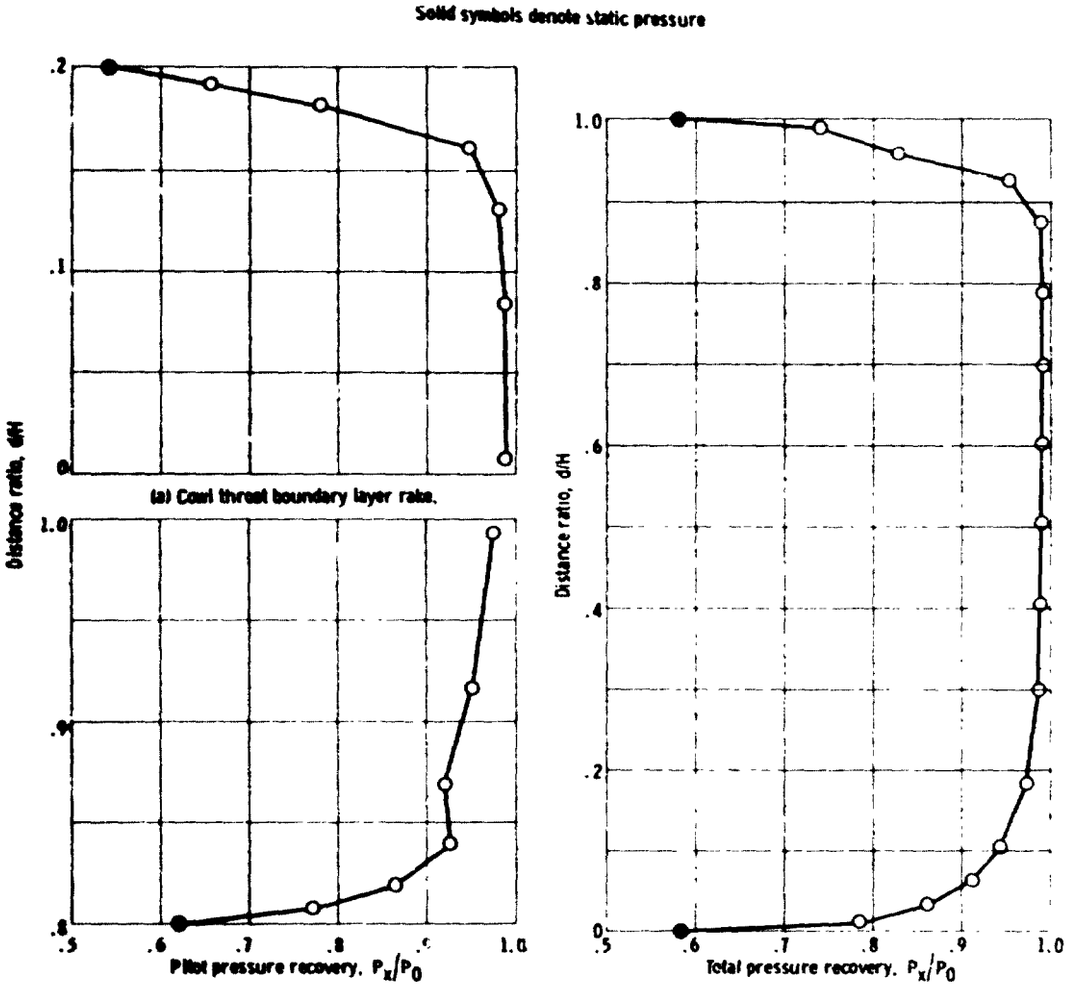

Figure 13. - Total pressure profiles with set II vortex generators; configuration Accb; sealed bypass; area-weighted total pressure recovery, $\bar{P}_2/P_0$, 0.93; mass-flow ratio, m_2/m_0, 0.904; free-stream Mach number, M_0, 2.0; critical inlet operation.

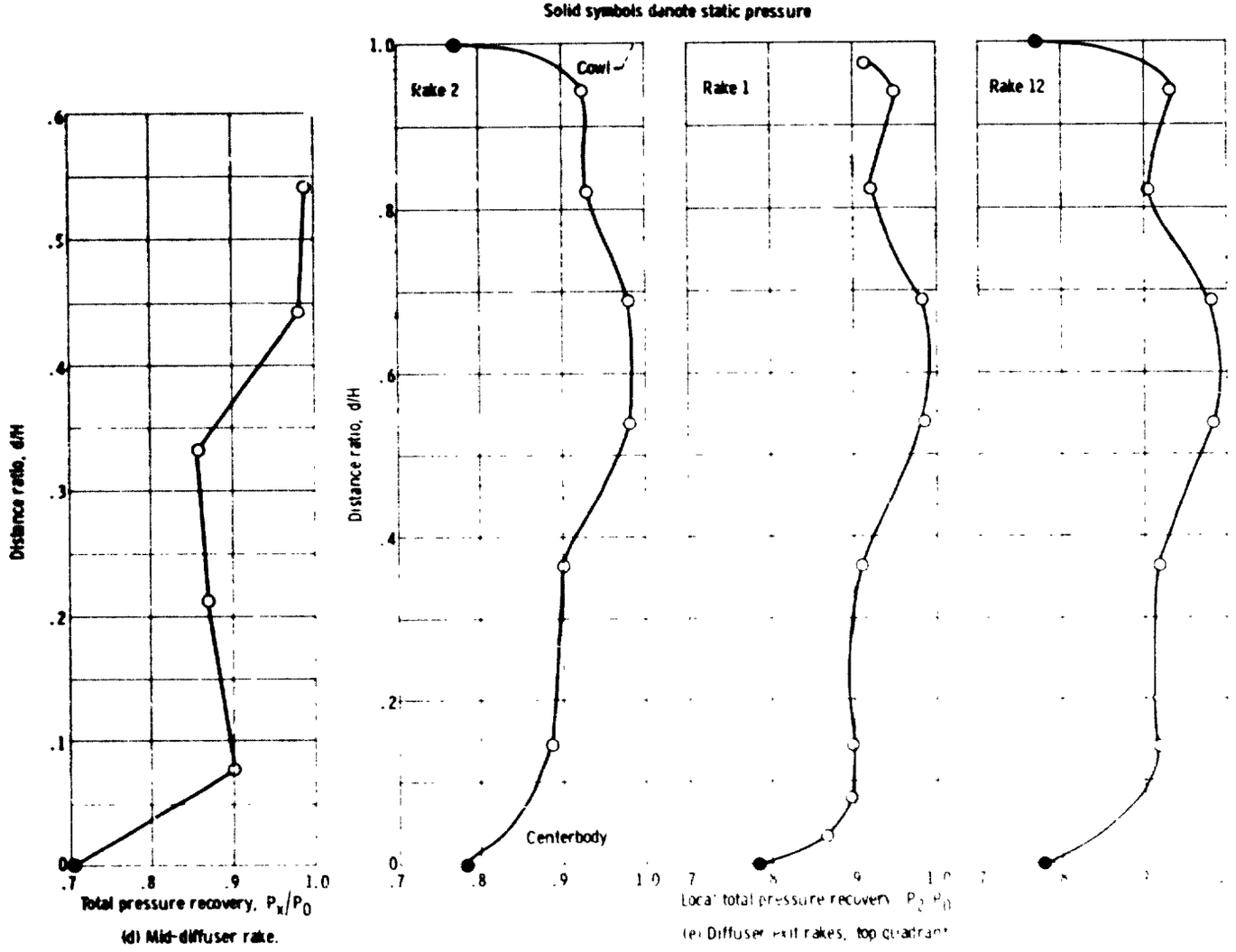

Figure 13. Concluded

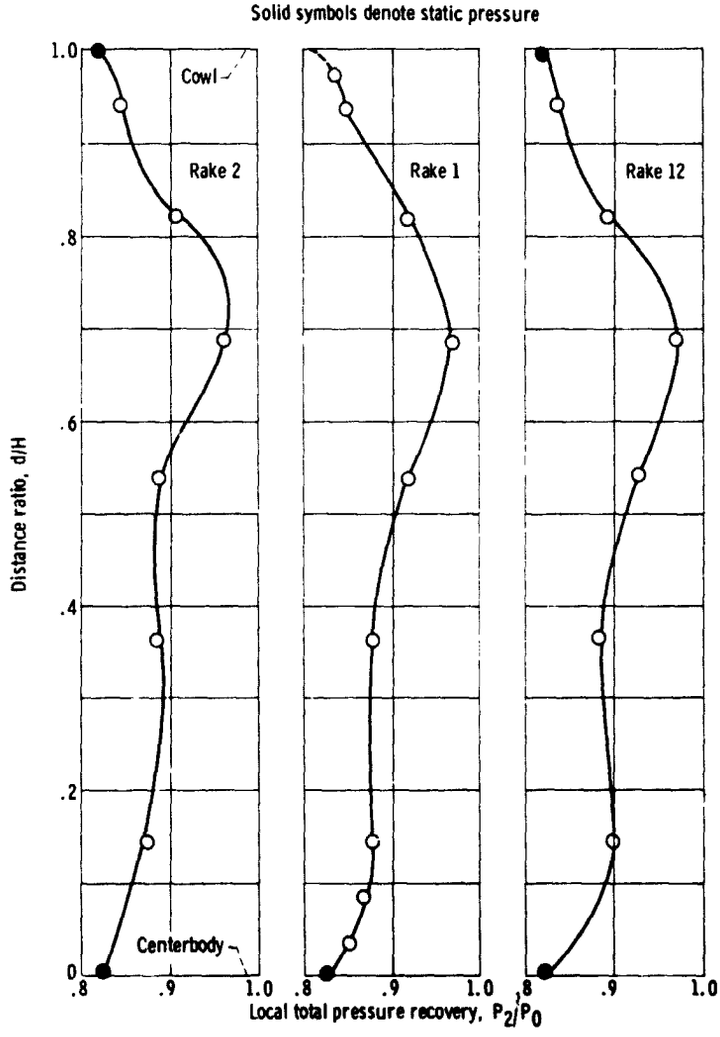

Figure 14. - Total pressure profiles of diffuser exit rakes (top quadrant) with set II vortex generators; configuration Acb; sealed bypass; area-weighted total pressure recovery, $\bar{P}_2/P_0$, 0.899; mass-flow ratio, m_2/m_0, 0.980; free-stream Mach number, M_0, 2.5; critical inlet operation.

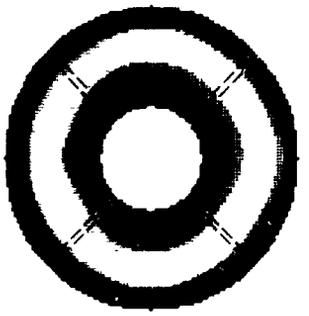

(a) Without vortex generators; configuration A; area-weighted total pressure recovery, $\bar{P}_2/P_0$, 0.886; mass-flow ratio, m_2/m_0, 0.981; free-stream Mach number, M_0, 2.5.

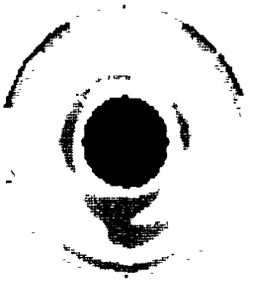

(b) With set I vortex generators; configuration Dccb; area-weighted total pressure recovery, $\bar{P}_2/P_0$, 0.900; mass-flow ratio, m_2/m_0, 0.974; free-stream Mach number, M_0, 2.5.

(c) With set II vortex generators; configuration Accb; area-weighted total pressure recovery, $\bar{P}_2/P_0$, 0.899; mass-flow ratio, m_2/m_0, 0.977; free-stream Mach number, M_0, 2.5.

(d) With set II vortex generators; configuration Acb; area-weighted total pressure recovery, $\bar{P}_2/P_0$, 0.899; mass-flow ratio, m_2/m_0, 0.980; free-stream Mach number, M_0, 2.5.

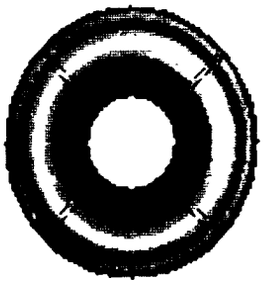

(e) With set II vortex generators; configuration Accb; area-weighted total pressure recovery, $\bar{P}_2/P_0$, 0.938; mass-flow ratio, m_2/m_0, 0.904; free-stream Mach number, M_0, 2.0.

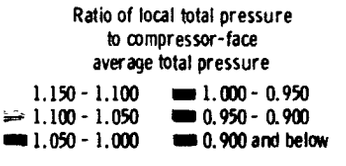

Figure 15. - Diffuser exit total pressure contours for critical inlet operation with sealed bypass system.

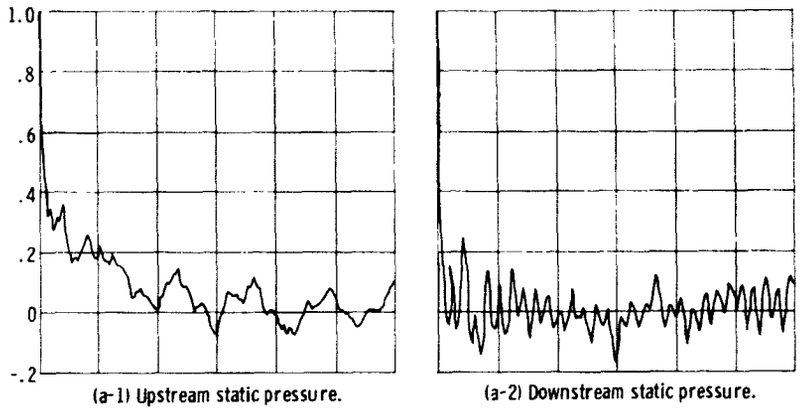

(a-1) Upstream static pressure. (a-2) Downstream static pressure.

(a) Without vortex generators; configuration A; area-weighted total pressure recovery, $\bar{P}_2/P_0$, 0.886; mass-flow ratio, m_2/m_0, 0.981.

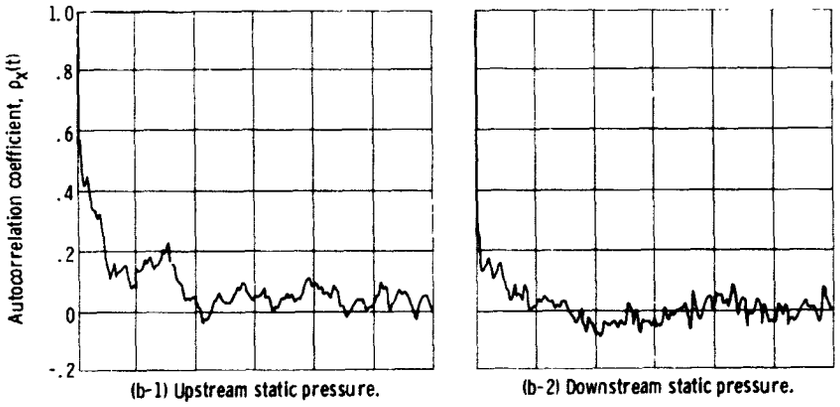

(b-1) Upstream static pressure. (b-2) Downstream static pressure.

(b) With set II vortex generators; configuration Accb; area-weighted total pressure recovery, $\bar{P}_2/P_0$, 0.899; mass-flow ratio, m_2/m_0, 0.977.

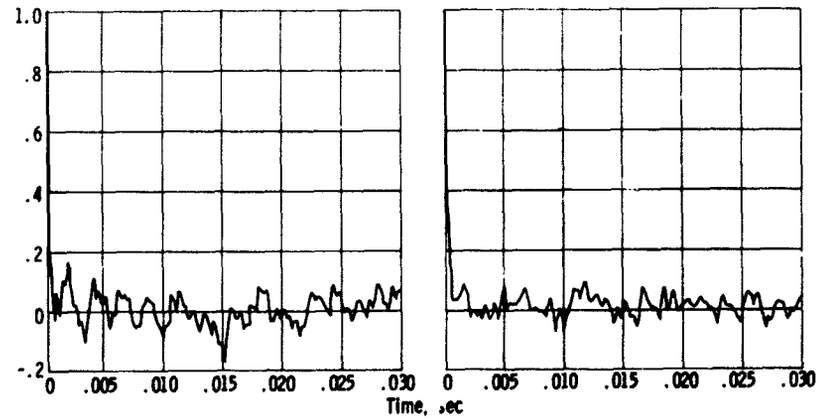

(c-1) Without vortex generators; configuration A; area-weighted total pressure recovery, $\bar{P}_2/P_0$, 0.886; mass-flow ratio, m_2/m_0, 0.981.

(c-2) With set II vortex generators; configuration Accb; area-weighted total pressure recovery, $\bar{P}_2/P_0$, 0.899; mass-flow ratio, m_2/m_0, 0.977.

(c) Diffuser exit total pressure.

Figure 16. - Autocorrelation coefficients of fluctuating component of wall static pressure upstream and downstream of vortex generators and diffuser exit total pressure. Sealed bypass; free-stream Mach number, M_0, 2.5; critical inlet operation.

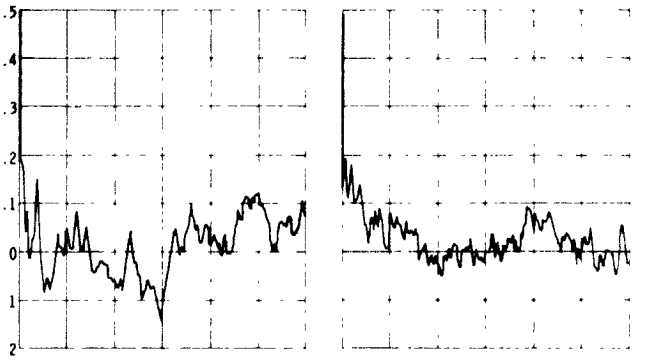

(a-1) Without vortex generators; configuration A; area-weighted total pressure recovery, $\bar{P}_2/P_0$, 0.886; mass-flow ratio, m_2/m_0, 0.981

(a-2) With set II vortex generators, configuration Accb; area-weighted total pressure recovery, $\bar{P}_2/P_0$, 0.899; mass-flow ratio, m_2/m_0, 0.977

(a) Cross-covariance of downstream static pressure with upstream static pressure. Downstream signal lags upstream signal.

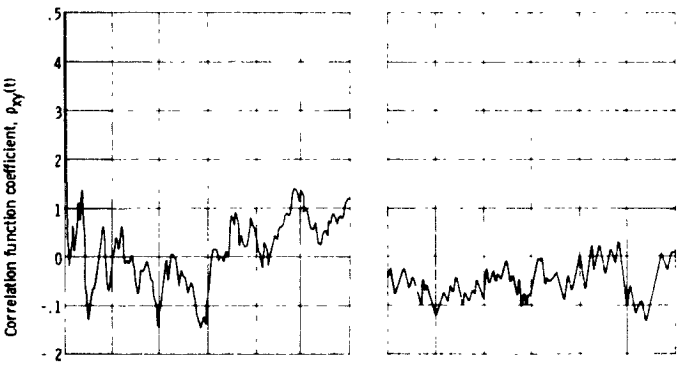

(b-1) Without vortex generators, configuration A; area-weighted total pressure recovery, $\bar{P}_2/P_0$, 0.886; mass-flow ratio, m_2/m_0, 0.981.

(b-2) With set II vortex generators, configuration Accb; area-weighted total pressure recovery, $\bar{P}_2/P_0$, 0.899; mass-flow ratio, m_2/m_0, 0.977.

(b) Cross-covariance of diffuser exit total pressure with upstream static pressure. Diffuser exit signal lags upstream signal.

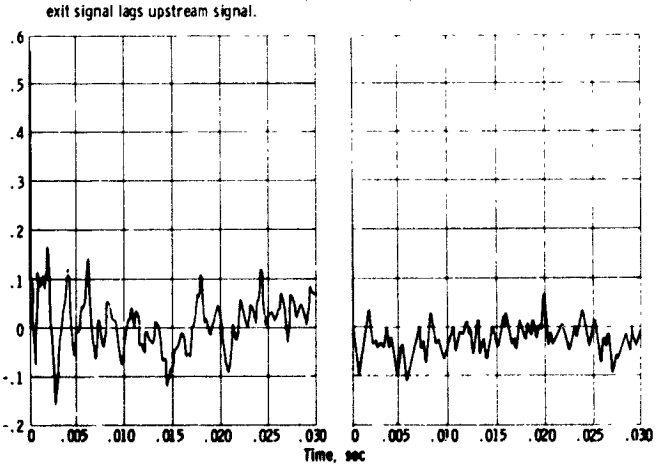

(c-1) Without vortex generators; configuration A; area-weighted total pressure recovery, $\bar{P}_2/P_0$, 0.886; mass-flow ratio, m_2/m_0, 0.981.

(c-2) With set II vortex generators; configuration Accb; area-weighted total pressure recovery, $\bar{P}_2/P_0$, 0.899; mass-flow ratio, m_2/m_0, 0.977.

(c) Cross-covariance of diffuser exit total pressure with downstream static pressure. Diffuser exit signal lags downstream signal.

Figure 17. - Correlation function coefficients (normalized cross-covariance function) of fluctuating component of two wall static pressures and diffuser exit total pressure. Sealed bypass; free-stream Mach number, M_0, 2.5; critical inlet operation.